DOT/FAA/AR-11/21

Federal Aviation Administration
William J. Hughes Technical Center
Aviation Research Division
Atlantic City International Airport
New Jersey 08405

Crushing Behavior of a Composite Corrugated Specimen Representative of an Aircraft Subfloor: Experiment and Simulation

September 2013

Final Report

U.S. Department of Transportation
Federal Aviation Administration

NOTICE

This report is available at the Federal Aviation Administration William J. Hughes Technical Center's Full-Text Technical Reports page: actlibrary.tc.faa.gov in Adobe Acrobat portable document format (PDF).

Technical Report Documentation Page

1. Report No.	2. Government Accession No.	3. Recipient's Catalog No.
DOT/FAA/AR-11/21		

4. Title and Subtitle	5. Report Date
CRUSHING BEHAVIOR OF A COMPOSITE CORRUGATED SPECIMEN REPRESENTATIVE OF AN AIRCRAFT SUBFLOOR: EXPERIMENT AND SIMULATION	September 2013
	6. Performing Organization Code

7. Author(s)	8. Performing Organization Report No.
Paolo Feraboli and Bonnie Wade	

9. Performing Organization Name and Address	10. Work Unit No. (TRAIS)
Automobili Lamborghini Advanced Composite Structures Laboratory Department of Aeronautics and Astronautics University of Washington Seattle, WA 98195-2400	11. Contract or Grant No.

12. Sponsoring Agency Name and Address	13. Type of Report and Period Covered
U.S. Department of Transportation Federal Aviation Administration William J. Hughes Technical Center Aviation Research Division Aircraft Systems & Structures Branch Atlantic City International Airport, NJ 08405	14. Sponsoring Agency Code AIR-100

15. Supplementary Notes

The Federal Aviation Administration William J. Hughes Technical Center Aviation Research Division Technical Monitor was Allan Abramowitz.

16. Abstract

This report investigates the ability of a commercially available, mainstream industry analytical tool to predictively simulate composites under crash conditions. Quasi-static crush tests of corrugated specimens manufactured with carbon fiber/epoxy prepreg tape were performed to measure the energy absorption of the material and specimen combination, and to validate the analytical model. The corrugated shape is representative of subfloor crashworthy structures, as used in general aviation and rotorcraft. A finite element model was generated using the commercially available explicit software LS-DYNA and the built-in progressive failure material model MAT54. This material model has been extensively used by the aircraft industry to simulate composite materials undergoing progressive damage under crash conditions as well as other foreign object impact scenarios. Reasonable agreement between simulation and experiment was obtained. Through a sensitivity study, the modeling strategy's strengths and shortcomings were identified. From this investigation, it was evident that this modeling approach cannot be considered truly predictive. The implications are that the element-level tests should be used for model calibration and not validation, within the certification strategy by analysis supported by test evidence.

17. Key Words	18. Distribution Statement
Crashworthiness, Energy absorption, Finite element modeling, Impact, Damage modeling, Carbon fiber	This document is available to the U.S. public through the National Technical Information Service (NTIS), Springfield, Virginia 22161. This document is also available from the Federal Aviation Administration William J. Hughes Technical Center at actlibrary.tc.faa.gov.

19. Security Classif. (of this report)	20. Security Classif. (of this page)	21. No. of Pages	22. Price
Unclassified	Unclassified	57	

ACKNOWLEDGEMENTS

The authors would like to thank Dr. Mostafa Rassaian and his advanced analysis team: Alan Byar, Michael Rucki, and Mark Higgins. Dr. Rassaian was instrumental in establishing the LS-DYNA modeling capabilities at University of Washington and strengthening the ongoing projects concerned with crash simulation.

The authors would also like to thank Dr. Xinran Xiao (previously at General Motors, now at Michigan State University) for guidance with fundamentals of the explicit finite element modeling, as well as the active members of the Crashworthiness Working Group of the Composite Materials Handbook-17 (CMH-17 formerly MIL-HDBK-17); Paul Robertson and Aeronautical Test Services (ATS) of Arlington, WA, for providing the mold design and manufacturing; Andrea Dorr and Leslie Cooke (Toray Composites) for donating the prepreg materials.

TABLE OF CONTENTS

LIST OF FIGURES

LIST OF TABLES

LIST OF ACRONYMS

CDM	Continuum damage mechanics model
CFC	Channel frequency class
CMH-17	Composite Materials Handbook, formerly MIL-HDBK-17
DLR	German Aerospace Agency
EA	Energy absorbed (the total area under the load-displacement curve)
EFS	Effective failure strain
FAA	Federal Aviation Administration
FBRT	Softening factor for fiber tensile strength after matrix failure
FE	Finite element
FEM	Finite element model
LP	Load-penetration (curve for LS-DYNA contact formulation)
PCWL	Piecewise linear
PFM	Progressive failure model
RN2RB	Rigid Nodes to Rigid Body
SC	Shear strength
SEA	Specific energy absorption (the energy absorbed per unit mass of crushed structure)
SOFT	Softening factor for crashfront elements experiencing crash load
TFAIL	Minimum time step size criteria for element deletion
XC	Longitudinal compressive strength
XT	Longitudinal tensile strength
YC	Transverse compressive strength
YCFAC	Softening factor for fiber compressive strength after matrix failure
YT	Transverse tensile strength

EXECUTIVE SUMMARY

The behavior of composite materials under crash conditions poses particular challenges for engineering analysis since it requires modeling beyond the elastic region and into failure initiation and propagation. Crushing is a combination of several failure mechanisms, such as matrix cracking and splitting, delamination, fiber tensile fracture and compressive kinking, frond formation and bending, and friction. Even with today's computational power, it is not possible to capture each of the failure mechanisms; hence, simplifications are required. Macro-mechanical models based on lamina-level properties have been used, notwithstanding the well-accepted limitations for composite failure criteria in predicting the onset of damage within laminate codes. The ability of a commercially available, mainstream industry analytical tool to predictively simulate composite structures under crash conditions was investigated.

This report contains the results of element-level experiments, consisting of the quasi-static crushing of corrugated specimens manufactured with carbon fiber/epoxy prepreg tape. The tests were performed to measure the specific energy absorption and validate the numeric simulation. The corrugated shape is representative of subfloor crashworthy structures used in general aviation and rotorcraft. The corrugated geometry is also appealing from a test perspective since it is self-supporting (i.e., it does not require a stabilizing fixture), it does not feature hoop tensile stress phenomena typical of tubular structures, and it is easy to manufacture.

This report also includes a detailed explanation of the modeling approach used to simulate the crush test. A finite element model was generated using the commercially available explicit software LS-DYNA. The built-in progressive failure material model MAT54 was successfully used to obtain agreement with the experiment results. Material model MAT54 has been extensively used by the aircraft industry to simulate composite materials undergoing progressive damage under crash conditions as well as other foreign object impact scenarios.

Through a sensitivity study, the modeling strategy's strengths and shortcomings were identified. Several modeling parameters, which have no physical meaning or cannot otherwise be measured experimentally, have a strong influence on the success of the simulation. For example, the SOFT crashfront parameter is the single most influential parameter for determining the success of the simulation. These parameters need to be calibrated by trial and error to match the experimental results; hence, it cannot be determined a priori. From this investigation, it became evident that this modeling approach cannot be considered to be truly predictive. The implications are that the element-level tests (e.g., the crushing of an energy-absorbing component, such as the corrugated specimen) should be used for model calibration and not validation, within the certification strategy by analysis supported by test evidence. Once the model is calibrated at this level, the analysis model can be used at the higher levels of complexity to predict the crash response of subcomponents, components, and full-scale test articles.

1. INTRODUCTION.

The objective of designing aircraft for crashworthiness is to reduce injuries and fatalities [1]. No single component of the aircraft can, by itself, protect the occupant from the extreme accelerations that can occur during a crash; rather, all the various components must act in unison to provide a crashworthy response. Specifically, crashworthiness encompasses both the design of the primary aircraft structure and the auxiliary systems (e.g., seats, restraint systems, overhead luggage bins, fire suppression systems, etc.). To optimize the crashworthy design of the structure, it is necessary to provide a crash-resistant, protective shell surrounding the occupants and to incorporate strategically positioned, load-limiting, energy-absorbing components [2-24]. These energy-absorbing components are specifically designed to dissipate kinetic energy under controlled collapse. Typical energy absorbers in passenger aircraft include subfloor stanchions and floor beams [2-17]. These structural components have a similar function to the nose cone, side, and rear impact structures in open-wheel racecars [18-20] and tubular front rails in the crumple zone of passenger cars [21-24]. While the total energy dissipated during a crash depends on the overall vehicle system deformation, the crash-oriented design of the individual energy-absorbing structural components of simple geometry can provide an increase in structural crashworthiness and survivability.

Corrugated beams have been employed as energy absorbers in the subfloors of aircraft to improve crashworthiness. The corrugation increases the stability of the web, thereby increasing its crippling strength and, hence, enables the floor beams to carry higher design loads. By reducing the likelihood of macroscopic buckling, the corrugated geometry also promotes stable crushing and significant energy absorption in case of a crash [25].

In the United States (U.S.), most of the crashworthiness research focus has been directed toward military rotorcraft through U.S. Army-sponsored research programs between the 1970s and late 1990s [2-4]. For example, the fuselage concepts developed during the Advanced Composite Aircraft Program (ACAP) [5-6] and, more recently, the Survivable Affordable Repairable Airframe Program [7] use a mix of frangible composite subfloor structures integral to the composite-intensive airframe (figure 1). These structures incorporated corrugated laminated composite webs, tubular and semitubular concepts, as well as honeycomb or foam sandwich approaches. During the same time period, the National Aeronautics and Space Administration and the Federal Aviation Administration (FAA) were involved in extensive research to characterize the advantages of retrofitting general aviation aircraft with crashworthy features [8], for example, using corrugated composite webs in the floor beams (figure 2).

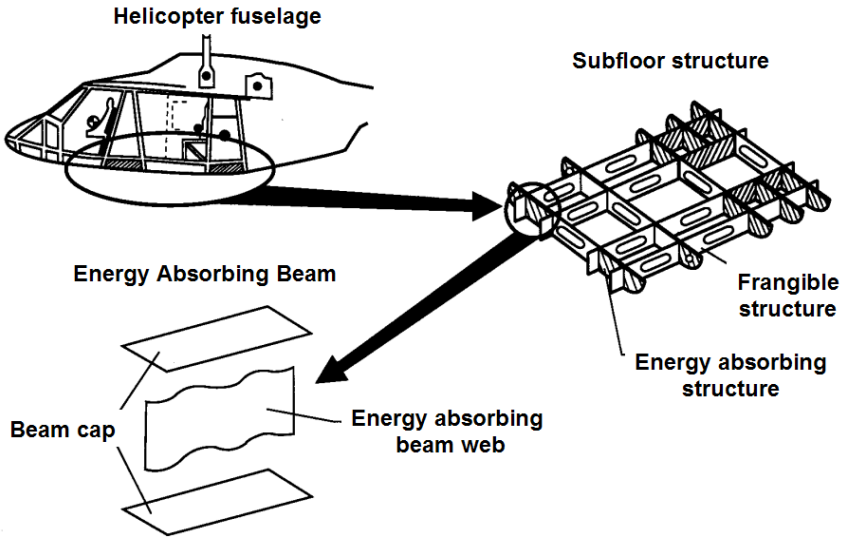

Figure 1. Frangible Corrugated Subfloor Structures

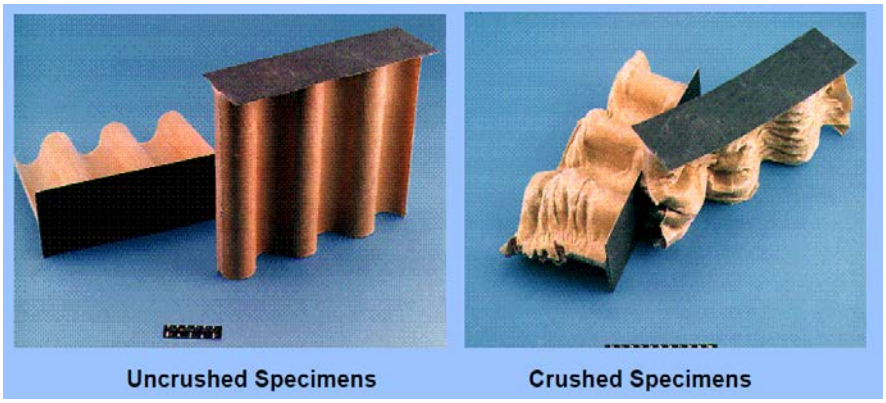

Figure 2. Corrugated Composite Webs Evaluated for Use as Floor Beams for General Aviation Aircraft

In the late 1990s, the European Union funded the Commercial Aircraft Design for Crash Survivability (CRASURV) program [9-14] that promoted the design, fabrication, and testing of crashworthy composite airframe components. Under this program, the German Aerospace Center (DLR) developed a corrugated composite, energy-absorbing subfloor box and finite element model (FEM) typical for rotorcraft and small commuter aircraft [9 and 10] (figure 3). Also under this program, the Dutch National Aerospace Laboratory (NLR) developed a corrugated composite, energy-absorbing curved aircraft subfloor structure and FEM typical for large commercial transport aircraft [12 and 13] (figure 4). The crashworthy subfloor designs shown in figures 1 and 2 have shown that corrugated composite components, which are designed to absorb significant amounts of energy during a crash, are feasible and effective in a crashworthy aircraft design.

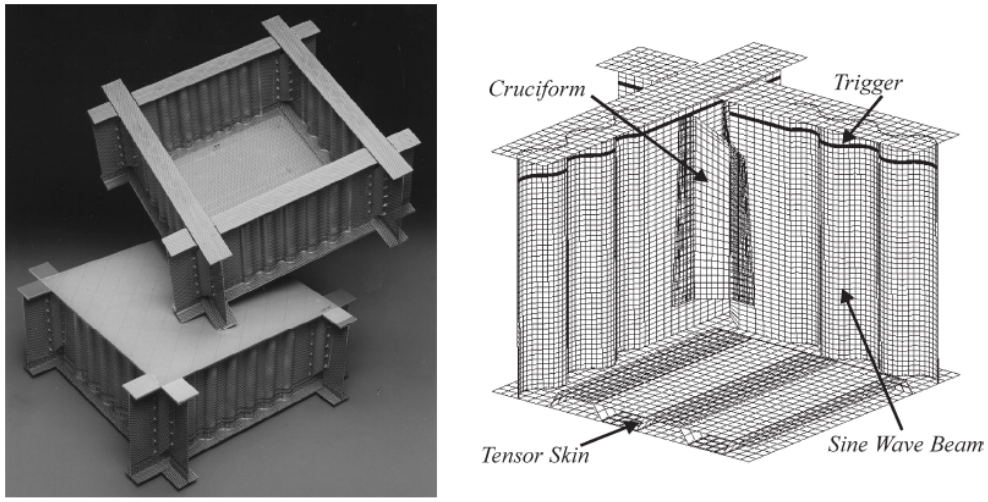

Figure 3. Models of Corrugated Composite, Energy-Absorbing Subfloor Box for Rotorcraft and Small Airplanes

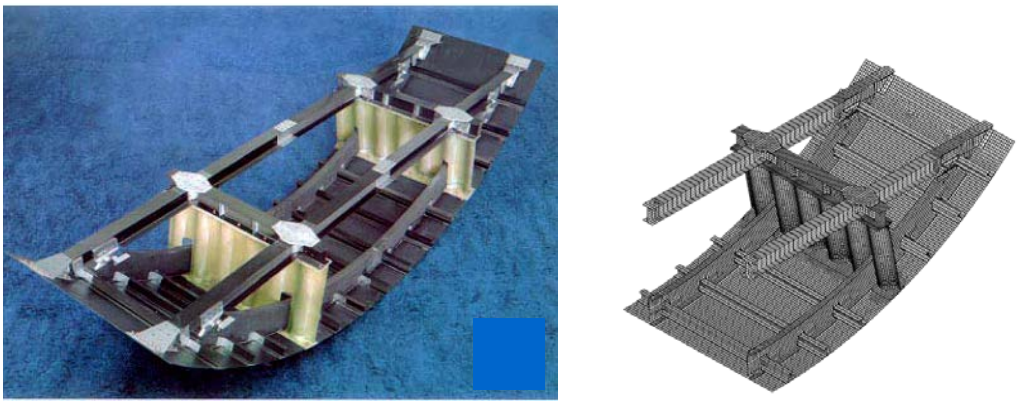

(a) (b)

Figure 4. Corrugated Composite, Energy-Absorbing Floor Beams for an Aircraft Subfloor Section, (a) Test Article and (b) FEM

The pre- and postcrush corrugated composite subfloor developed by DLR is shown in figure 5. Its effectiveness has been demonstrated through analysis supported by test evidence [10, 13, and 14]. Although it was possible to reproduce analytically the damage morphology and overall response of the subfloor observed during the experiment, the effort required calibrating the model a posteriori to match the experimental results. This led the researchers to conclude that the current analysis methods for composite crashworthiness are nonpredictive [10, 13, and 14].

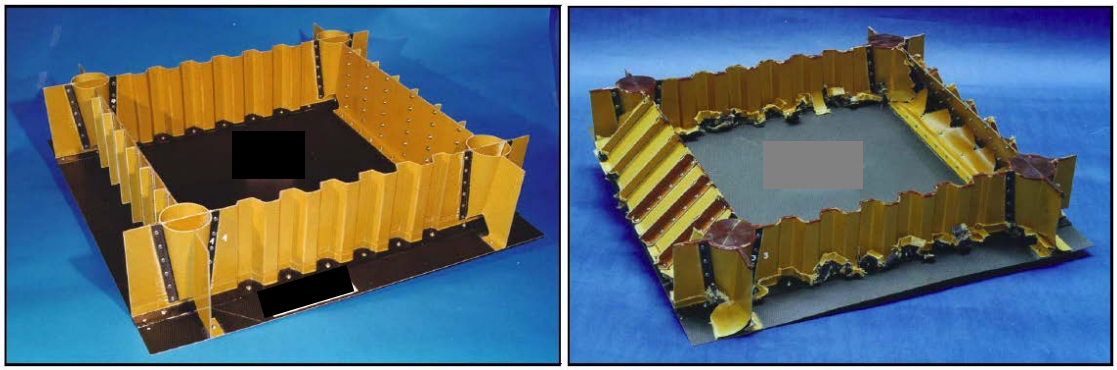

(a) (b)

Figure 5. Carbon and Kevlar Fiber Corrugated Subfloor Test Article
(a) Before and (b) After Crush

Based on these results, the research investigated the capability of current commercial mainstream analysis tools to successfully simulate the crash response of composite structures. A multiyear research program was developed to focus on

- establishing standardized test methods to measure energy absorption of composite materials and structures.
- developing guidelines for the successful analytical modeling of composites under crash conditions.
- generating guidance material for certification protocols based on analysis supported by test evidence.

Within the broader scope of this project, the research discussed in this report is aimed at determining the capability of a mainstream commercial finite element modeling tool to simulate the axial crushing response of a structural element of simple geometry, a corrugated carbon fiber-reinforced plastic web.

2. EXPERIMENT.

2.1 EXPERIMENTAL SETUP.

The material used in this study was a unidirectional tape prepreg developed by Toray Carbon Fibers America, Inc., for the general aviation industry, which was evaluated during the Advanced General Aviation Transport Experiments (AGATE) program. The Toray T700 carbon fiber was pre-impregnated with a 270°F-cure 2510 epoxy. The material properties for this material system are published in CMH-17 [1] and reproduced in appendix A. The lay-up was a 12-ply cross-ply $[0/90]_{3s}$, yielding an average laminate thickness of 0.07 in. The corrugated test specimens were manufactured by press-claving (or press molding) through a set of aluminum matched tools (figure 6) [26 and 27]. The molds feature alignment pins for accurate positioning.

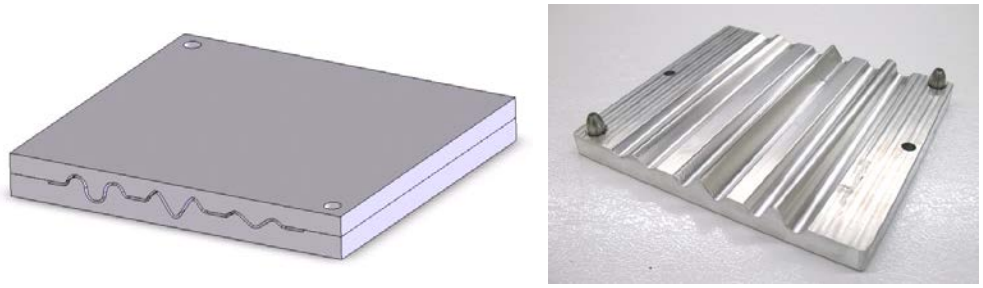

Figure 6. Matched Aluminum Mold for Corrugated Test Specimen

The corrugated geometry features a 0.25-in.-radius semicircular segment repeated three times at alternating sides with respect to the midplane (figure 7). This coupon has straight end-lips of material on each side of the corrugation for additional stability. Each specimen was machined from the molded panel and was further chamfered with a single-sided 45° chamfer (figure 8). Each coupon measured 3.0 in. long and 2.0 in. wide from end-lip to end-lip.

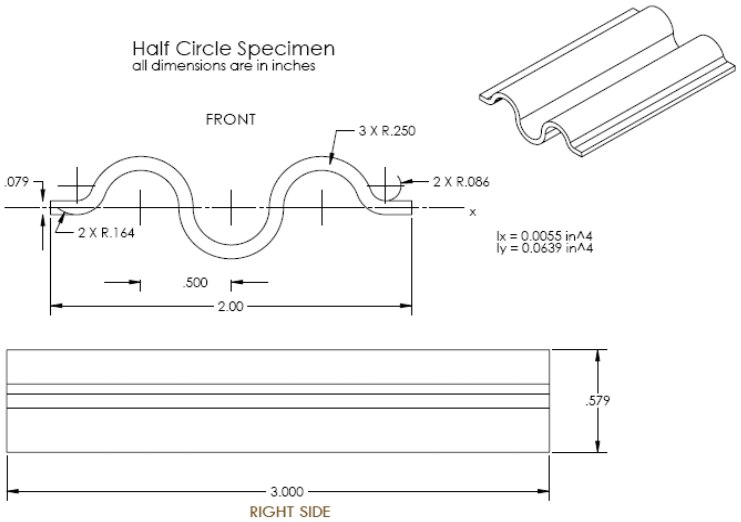

Figure 7. Detailed Geometry of the Corrugated Test Specimen

Figure 8. Corrugated Test Specimen With 45° Single-Sided Chamfer Trigger

The specimens, which are self-supporting and do not require additional stabilization [25-29], were tested under quasi-static uniaxial crushing. The test fixture is comprised of two flat steel plates, the base plate, and the load plate. The specimen rests vertically between the two plates, with the triggered end unsupported on the base plate (figure 9). Four posts with linear bearings were used to keep the plates aligned with respect to each other, and a self-aligning steel sphere was used to introduce the load from the crosshead into the load plate. Tests were conducted at a crosshead displacement rate of 2.0 in./min in an electromechanical universal test frame under displacement control. During the test, the load and crosshead displacement values were recorded. Five specimens were tested for repeatability.

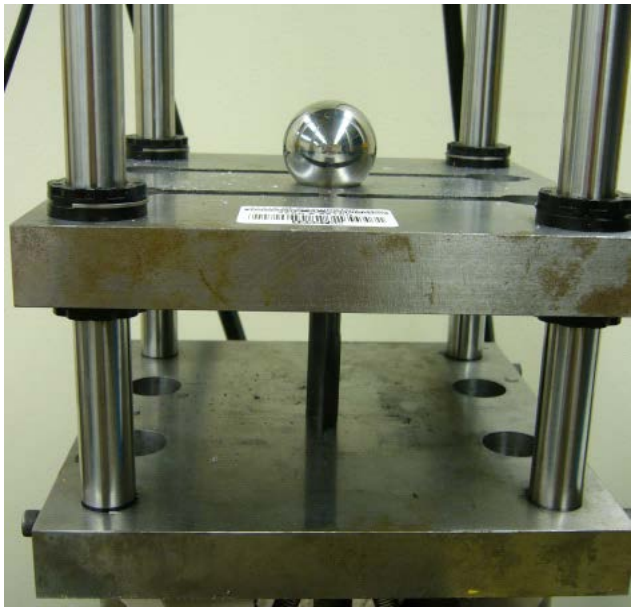

Figure 9. Test Fixture With Specimen Installed

2.2 EXPERIMENTAL RESULTS.

The ability of a material to absorb energy can be expressed in terms of specific energy absorption (SEA), defined as the energy absorbed (EA) per unit mass of crushed structure. The energy absorbed is calculated as the total area under the force-stroke diagram (EA), while the mass of the structure that undergoes crushing is given by the product of stroke l, cross-sectional area A, and density ρ:

$$SEA = \frac{EA}{\rho \cdot A \cdot l} = \frac{\int F \cdot dl}{\rho \cdot A \cdot l} = \frac{F_{avg}}{\rho \cdot A} \tag{1}$$

where F is the instantaneous crush force, and F_{avg} is the sustained crush force, which is the displacement-average value of the crush force and a direct indicator of the energy absorbed. The SEA is typically measured in J/g or kJ/kg units. The SEA is a well-accepted parameter used to quantify the ability of the material and structure to absorb energy.

The corrugated geometry was successful in achieving stable, sustained crushing associated with high-energy absorption. Crush progression is shown in figure 10 (a-f), and the experimental plots for load, SEA, and total EA as a function of crosshead displacement during each crush test are shown in figure 11 (a-c). The final damage morphology shows the formation of long fronds on the outer 0° plies and fragmentation of the inner 0° and all 90° plies, as shown in figure 12. After the test, significant amounts of carbon fiber and resin debris are left on the base plate (figure 13).

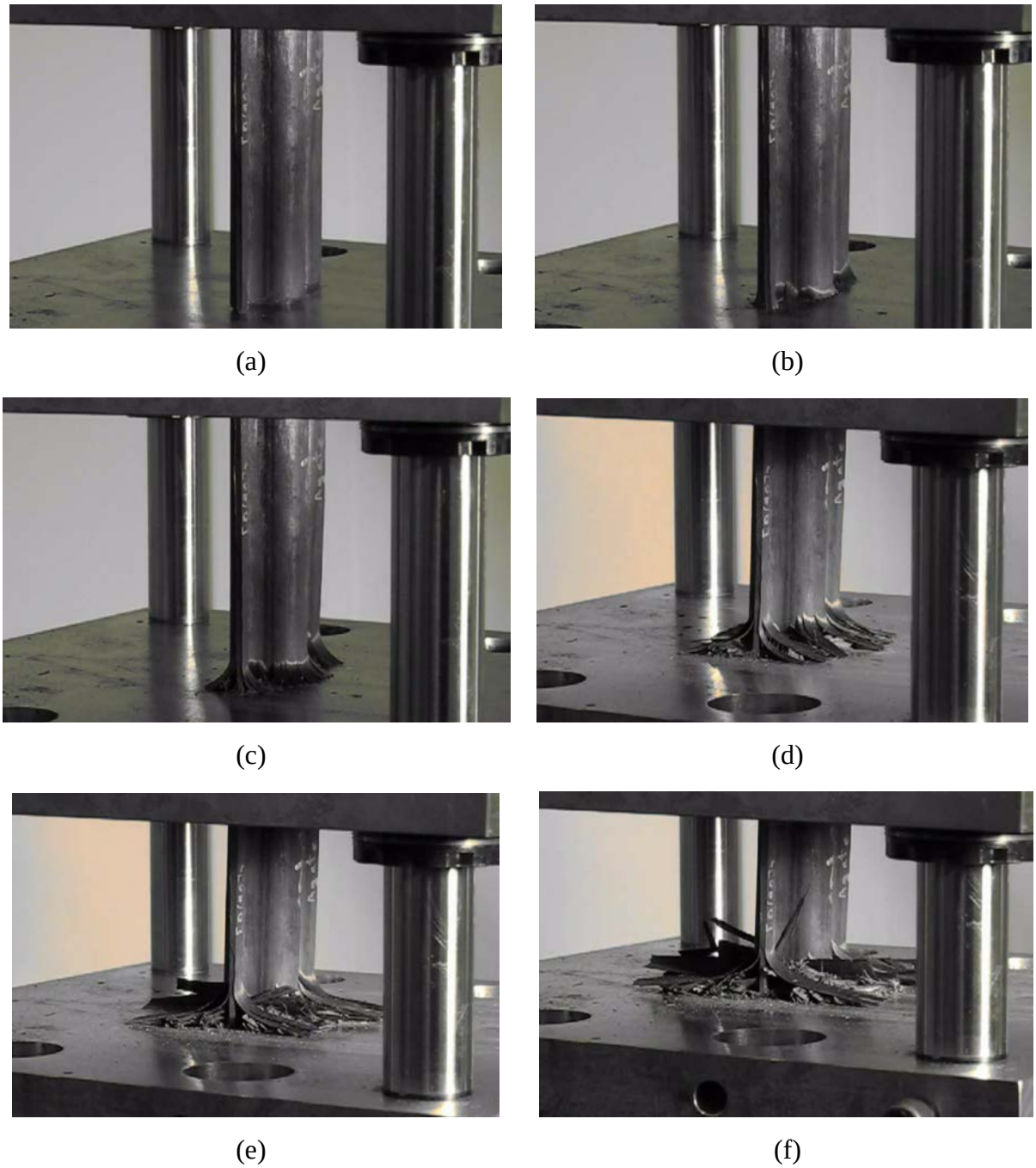

(a) (b)

(c) (d)

(e) (f)

Figure 10. Experimental Crush Progression

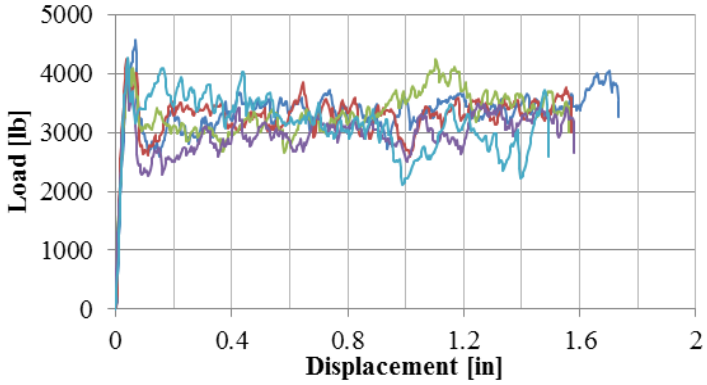

(a)

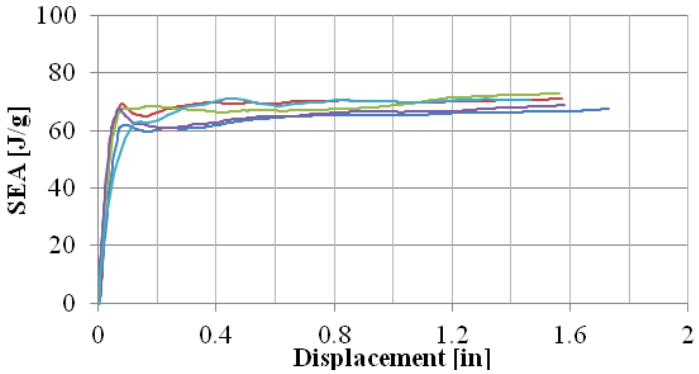

(b)

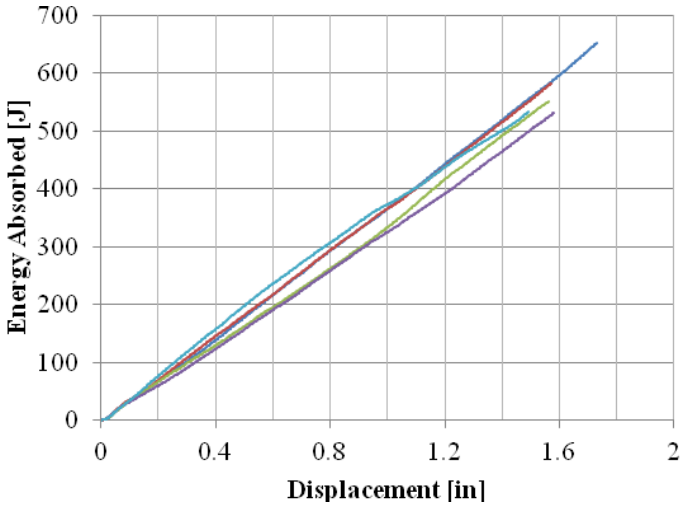

(c)

Figure 11. (a) Load, (b) SEA, and (c) Total EA Plots as a Function of Displacement During the Five Crush Experiments

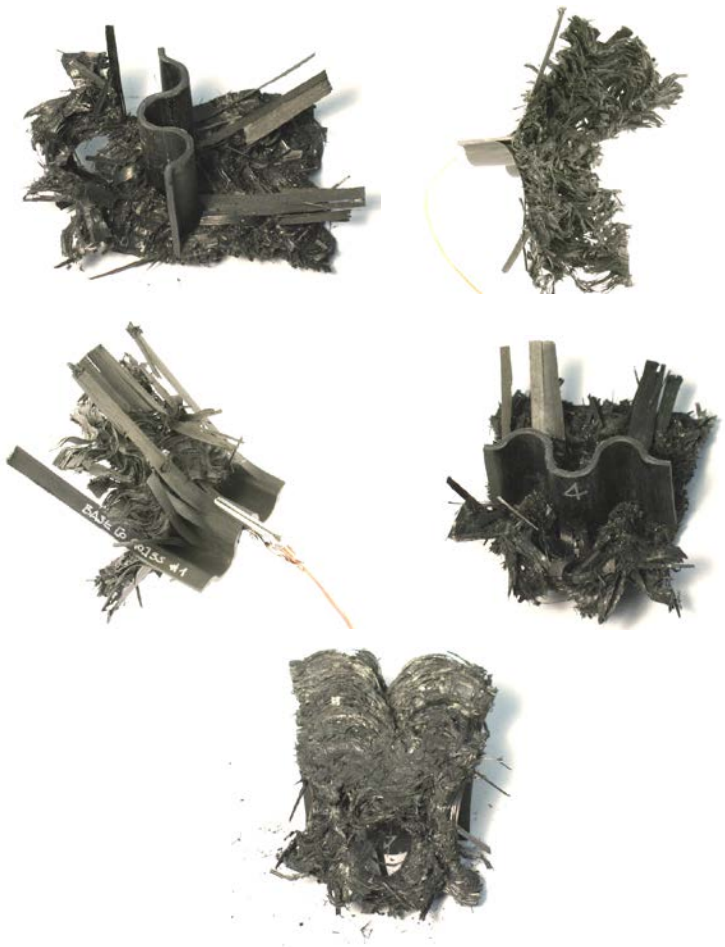

Figure 12. Representative Crushed Corrugated Specimens Showing Fragmentation Failures

Figure 13. Carbon Fiber/Epoxy Dust and Debris Left in the Test Fixture Following a Crush Test

Using the load and displacement data recorded during the test, the SEA value was calculated using equation 1 for each specimen tested. Good repeatability was observed among the five specimens, as the average SEA was 67.06 J/g with only a 4% Coefficient of Variance (CoV) and a standard deviation of less than 2.5 J/g.

3. ANALYTICAL MODEL.

3.1 CHALLENGES.

The introduction of composites in the primary structure of modern aircraft presents special challenges for the designer dealing with crashworthiness. The high SEA of composite materials is appealing for crash energy management, and composites can offer improved crashworthiness over their metallic counterparts if properly engineered. However, the energy-absorbing behavior of composites is not easily predicted due to the complexity of the failure mechanisms that can occur simultaneously within the material during a crash. These mechanisms include fiber tensile fracture and compressive kinking, matrix cracking and splitting, fiber-matrix debonding, and delamination. In addition, the overall crush response is highly dependent on a number of parameters (e.g., geometry, material system, lay-up, and impact velocity), which are not easily captured by analysis.

Although it is possible to develop a model that accurately reproduces experimental crush results, the simulation is highly sensitive to changes in model parameters, many of which cannot be measured experimentally or have no immediate physical meaning. Achieving successful simulation results for composite crushing requires extensive calibration of these parameters by trial and error and a profound understanding of the strengths and challenges of the selected modeling strategy.

Among the challenges associated with composite crush simulations, modeling beyond the elastic region and into failure initiation and propagation is paramount. Using the currently available computational resources, it is not possible to capture each of the complex failure mechanisms that occur during the crushing of composite structures. Models based on lamina-level failure criteria have been used, although with accepted limitations [30] to predict the onset of damage within laminate codes. Once failure initiates, the mechanisms of failure propagation require reducing the material properties using several degradation schemes [31]. Dynamic impact analysis requires using an explicit finite element (FE) code (e.g., the central difference method [31]), which solves the equations of motion numerically by direct integration using explicit rather than standard methods. Commercially available FE codes commonly used for crash simulations include LS-DYNA, ABAQUS Explicit, RADIOSS, and PAM-CRASH [32]. For this investigation, LS-DYNA [33] was chosen to perform the dynamic crush simulations. LS-DYNA offers built-in material models for composites. Each material model uses a different modeling strategy that includes material properties, failure criterion, a material property degradation scheme, and usually a set of model-specific input parameters that are necessary for the computation but do not have a corresponding physical meaning.

Composites are modeled as orthotropic linear elastic materials within the failure surface, whose shape depends on the failure criterion adopted by the specific material model. Beyond the failure

surface, the appropriate elastic properties are degraded according to the degradation law. Depending on the specific degradation law used by the material model, the constitutive models can be divided into either progressive failure models (PFM) or continuum damage mechanics models (CDM). PFMs are appealing for their simplicity, since they require lamina-level input properties and are based on laminated mechanics failure theories. However, PFMs have limited flexibility in terms of damage progression, since the state of damage in a lamina goes from zero to unity in a single step, without discrete intervals. On the other hand, CDMs allow the user to define the degradation scheme in detail by specifying the unloading portion of the stress-strain curve and allow for damage to accumulate through progressive increments. CDMs also require the definition of additional parameters and often need additional test data that is difficult to gather. LS-DYNA offers a variety of material models for composite materials, which include both PFM (MAT22, MAT54, and MAT55) and CDM (MAT58 and MAT162).

Although many commercial FE codes and modeling strategies (material models) are available, this investigation was limited to one code (LS-DYNA) and one modeling strategy (material model MAT54). LS-DYNA material model MAT54 has been extensively used by the aircraft industry to simulate composite materials undergoing progressive damage under crash conditions as well as other foreign object impact scenarios [34-41]. The objective was to verify if the model, based solely on coupon-level material properties obtained from standard lamina-level material tests, could be used to predict the experimental crush test results of the corrugated structural element. Characteristics of the load-displacement curve (initial slope, peak load, average crush load, and overall stability) as well as the SEA value were used as metrics to compare the simulation to experimental results. Furthermore, through a detailed sensitivity study, the strengths and weaknesses of the chosen modeling strategy were determined. Parametric studies were performed on the MAT54 material properties, other MAT54 model-specific parameters, and modeling parameters that are not in the MAT54 definition, such as test velocity and mesh size.

3.2 THE MAT54 MATERIAL MODEL.

MAT54 is designed specifically to handle orthotropic materials such as unidirectional tape composite laminates. There are 40 parameters defined in the MAT54 material card, however, only 30 are active and used by the code. Active parameters include physical properties (density), elastic properties (moduli and Poisson's ratios), and failure properties (strengths and strains-to-failure). The material card entries for these parameters are obtained from the material properties available in CMH-17 [1] and are summarized in appendix A. Other model-specific parameters that have no corresponding physical meaning and cannot be measured experimentally are necessary for the simulation to progress in a stable fashion. These parameters include failure criterion parameters (ALPHA, BETA, TFAIL, and CRIT) and degradation scheme factors (FBRT, YCFAC, and SOFT). Definitions for the active 30 parameters are given in appendix B.

The elastic behavior and failure criterion of the MAT54 material model are described in the LS-DYNA Theory Manual, reproduced in appendix C. MAT54 uses the Chang-Chang failure criterion [27 and 28] to determine individual ply failure. The failure criterion is strength-based and uses a ply discount method to degrade material properties of the element as it experiences

failures in the plies. In this way, progressive failure is realized through ply-by-ply failure within the laminate, and once all the plies have failed, the element is deleted.

In addition to the strength-based Chang-Chang failure criteria [42], element deletion can also occur if the strains exceed the strains-to-failure (DFAILT, DFAILC, DFAILM, and DFAILS, defined in table B-1 in appendix B) for each ply. All strains-to-failure can be measured through coupon-level tests of the material. However, if they are not known, LS-DYNA allows a generic parameter to be used, effective failure strain (EFS), which acts as an approximate global failure strain. Effective strain is calculated using a weighted sum of the 1-, 2-, and 12-direction strains, as given by equation 2.

$$Effective\ Strain = \sqrt{\frac{4}{3}(\varepsilon_{11}{}^2 + \varepsilon_{11}\varepsilon_{22} + \varepsilon_{22}{}^2 + \varepsilon_{12}{}^2)} \tag{2}$$

where ε = strain

EFS is the value of effective strain corresponding to element failure. The EFS parameter is not truly a physical property and can only be estimated by trial and error.

Finally, element deletion may also occur if the minimum element time step, TFAIL, is exceeded. This option is useful in cases where the computational cost is driven up by highly distorted elements that no longer carry load but are not deleted from the prescribed element deletion criterion. These highly distorted elements require very small time steps; therefore, by defining a minimum allowed time step using TFAIL, these costly but useless elements can be eliminated.

There are three strength-reducing parameters defined within MAT54: FBRT, YCFAC, and SOFT. The FBRT and YCFAC strength reduction terms are used to degrade the pristine fiber strengths of the remaining plies for the compressive matrix failure. The strength degradation is applied using the following equations:

$$XT = XT^* * FBRT \tag{3}$$

where:

XT = longitudinal tensile strength
FBRT = softening factor for fiber tensile strength after matrix failure

$$XC = YC^* * YCFAC \tag{4}$$

where:

XC = longitudinal compressive strength
YC = transverse compressive strength
YCFAC = softening factor for fiber composite strength after matrix failure

Since FBRT is a strength reduction factor that uses the pristine strength as its multiplier, values within the range (0, 1) are admissible. YCFAC, however, uses YC as its multiplier to degrade XC, therefore, the admissible range for this parameter is (0, XC/YC), which, for this material system, is (0, 7.4).

The SOFT parameter reduces the strength of the elements immediately approaching the crashfront for crush loading. This parameter is used to avoid instabilities and ensure stable crushing when the load transitions from the active row of elements at the crashfront to the next row. If SOFT is set to unity (hence, 100% of the pristine strength is preserved), this sudden transition may lead to section buckling. Values of SOFT between (0, 1) represent a percentage reduction of strength, where SOFT = 0.6 would indicate that 60% of the pristine strength is preserved. SOFT is a multiplier for all strengths: XT, XC, transverse tensile strength (YT), YC, and shear strength (SC).

The input value for all three strength reduction parameters cannot be measured experimentally and needs to be determined through trial and error.

3.3 THE BASELINE MODEL.

The baseline LS-DYNA model (developed to model the crush progression of the corrugated coupon) is illustrated in figure 14, showing the loading plate, the corrugated composite specimen, and the trigger row of elements. The specimen was modeled with a total of 840 elements, meshed using a fully integrated 0.1-in. x 0.1-in.-square linear shell element (LS-DYNA formulation 16). The thickness of the specimen elements was 0.079 in., whereas the thickness of the crush trigger elements was reduced to 0.01 in. The specimen was kept at rest by constraining all degrees of freedom using a nodal single-point constraint boundary condition on the bottom row of nodes opposite the crush trigger. A large, single-shell element perpendicular to the specimen crashfront was used to model the loading plate and was given the material properties of steel using the built-in, rigid-body material model MAT20.

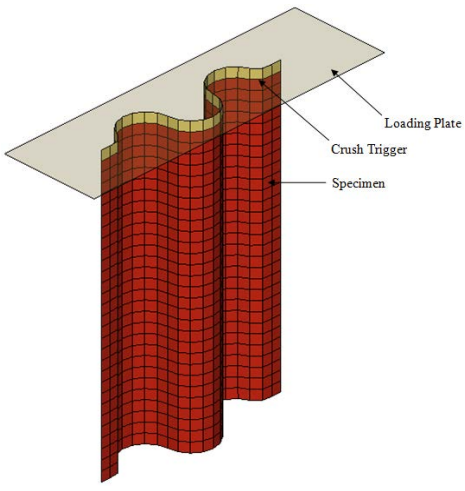

Figure 14. LS-DYNA Model of the Corrugated Composite Crush Specimen

The material stress-strain curves in the fiber (1) and matrix (2) directions are used as input parameters for the MAT54 material card. These curves, shown in figure 15, were generated using the material property values of the T700/2510 material system, given in appendix A.

The input deck for the baseline MAT54 material model is given in table 1.

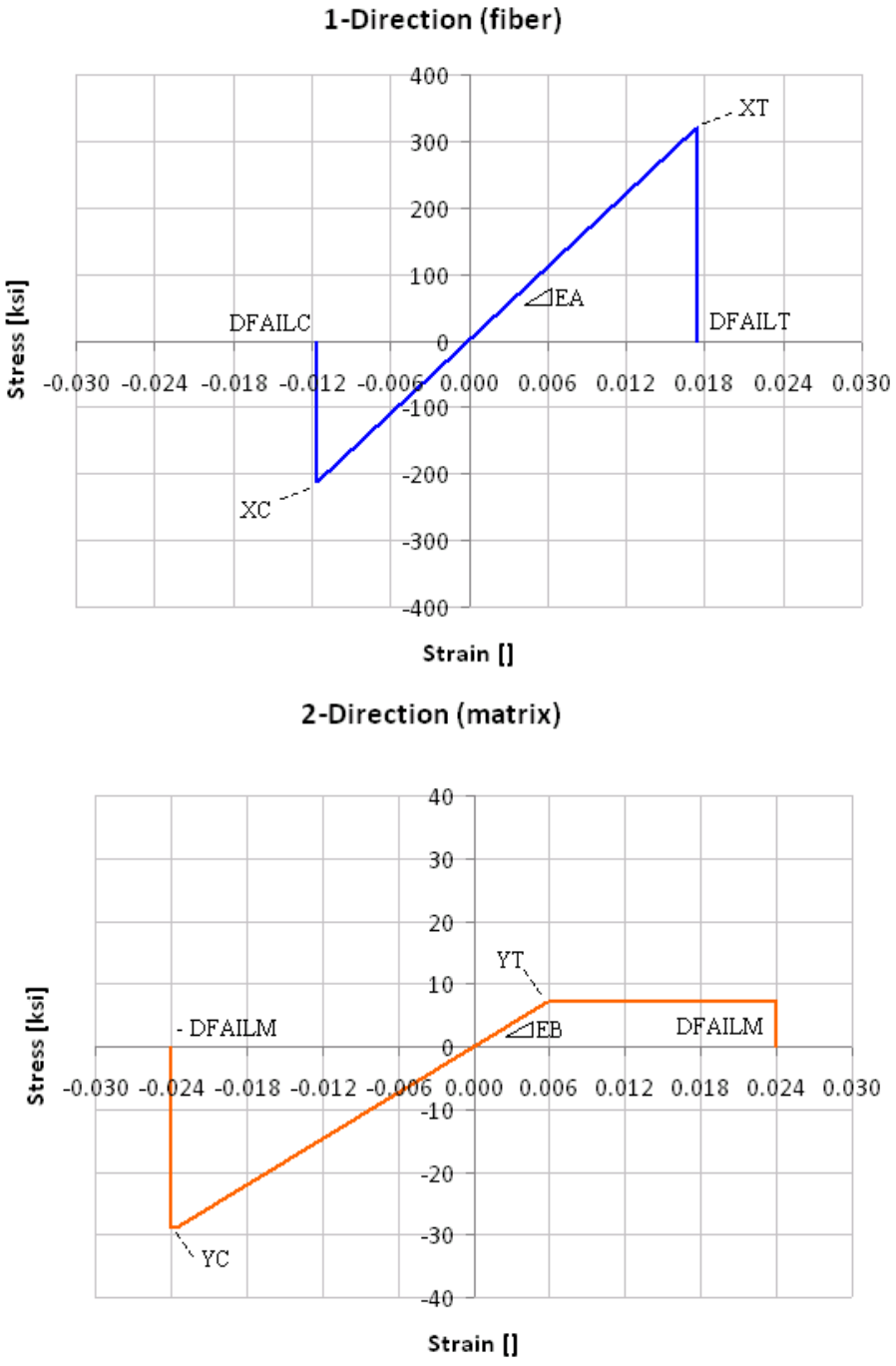

Figure 15. Material Stress-Strain Curves Generated by MAT54 Input Parameters

Table 1. The MAT54 Baseline Model Input Deck

MAT_054 (ENHANCED_COMPOSITE_DAMAGE)							
MID 1	RO 0.1500E-3	EA 0.1840E+8	EB 1220000	~~EC~~ 0.0	PRBA 0.02049	~~PRCA~~ 0.0	~~PRCB~~ 0.0
GAB 610000.0	GBC 610000.0	GCA 610000.0	~~KF~~ 0.0	AOPT 3.000	~~A1~~ 0.0	~~A2~~ 0.0	~~A3~~ 0.0
MANGLE 90.000	V1 0.0	V2 0.0	V3 1.000	~~D1~~ 0.0	~~D2~~ 0.0	~~D3~~ 0.0	
DFAILM 0.02400	DFAILS 0.03000	DFAILT 0.01740	DFAILC -0.01160	EFS 0.0	TFAIL 0.11530E-8		
ALPH 0.10000	SOFT 0.57000	FBRT 0.50000	YCFAC 1.200	BETA 0.50000			
XC 213000.0	XT 319000.0	YC 28800.00	YT 7090.000	SC 22400.00	CRIT 54.000		

Note: Parameters with a strikethrough are inactive and not used.

A contact definition between the loading plate and the specimen is necessary for the two parts to properly interact. LS-DYNA offers a variety of built-in contact algorithms. For crash analysis, standard penalty formulation contact methods are typically used [40 and 41]. Springs are placed normal to the surface between all penetrating nodes and the contact surface to facilitate a reaction force upon contact. The user input load-penetration (LP) curve defines the reaction normal force applied to each node as a function of the distance the node has penetrated through the surface that it is contacting. The baseline LP curve is shown in figure 16. The LP curve constitutes the most critical parameter for a given contact type and is discussed further in section 3.5.

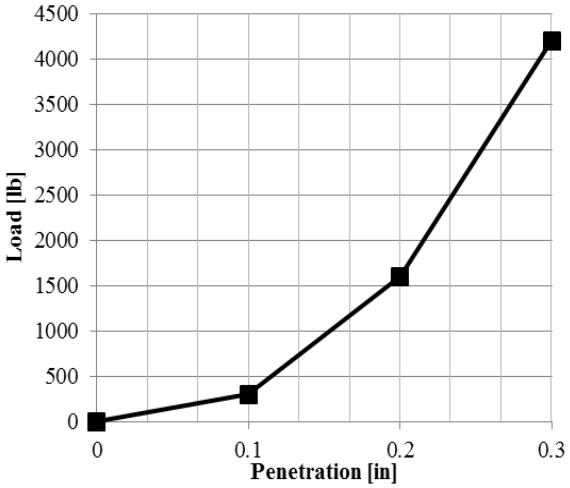

Figure 16. Load-Penetration Contact Curve Used by the Baseline Crush Simulation

The contact interface between the loading plate and the crush specimen was defined using the contact type "Entity" for the baseline simulation. This contact type requires that a virtual geometry or a shell-meshed geometry be defined as the master contact surface, which, in this case, was the shell loading plate.

The velocity of the loading plate was 150 in./sec, which was defined by a linear load curve imposed on the nodes of the loading plate. The effect of using a simulated crush velocity that is much higher than the experimental velocity is discussed in section 3.4.

The load-displacement crush curve obtained from the baseline model is shown in figure 17 in its raw and filtered state. The raw curve is characterized by sharp peaks and valleys resembling a saw-tooth pattern. This feature is a typical result of the mathematical model, which is linear up to failure at the peak, then drops to zero upon deletion of elements until the next element picks up the load again. It is common practice to filter the numeric results using a low-pass digital filter (SAE channel frequency class (CFC) 600) during postprocessing [28, 29, 32, 39, and 40]. Through filtering, the average crush load and SEA do not change, but the peaks and valleys are smoothed.

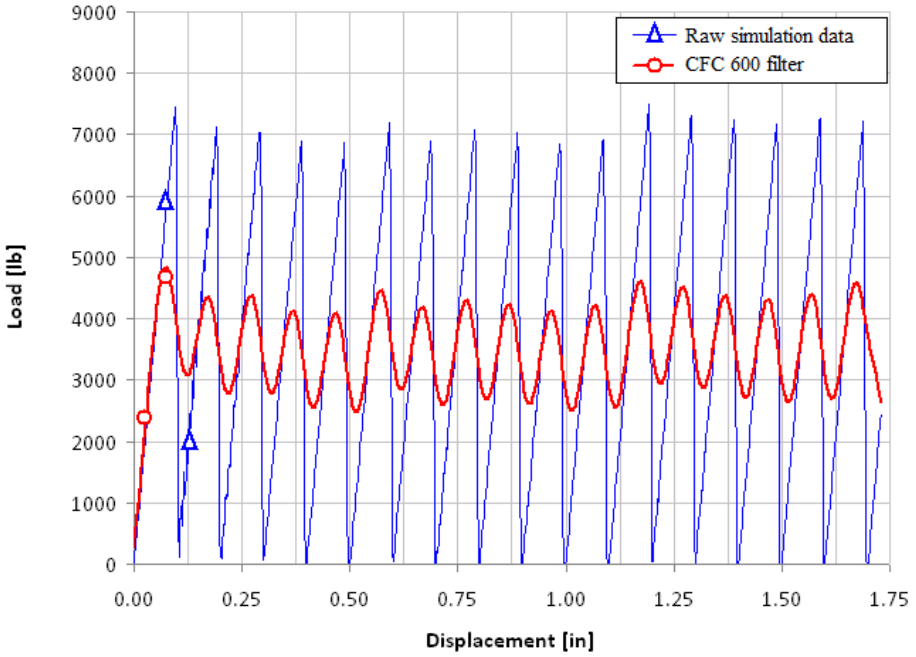

Figure 17. Raw and Filtered Numeric Crush Results From the Baseline Simulation

The filtered crush curve from the baseline simulation is compared with an experimental curve in figure 18. Only one of the experimental crush curves is shown for clarity. The filtered numeric curve oscillates about the average crush load without large variations in local peak values, indicating that the simulated crush is stable.

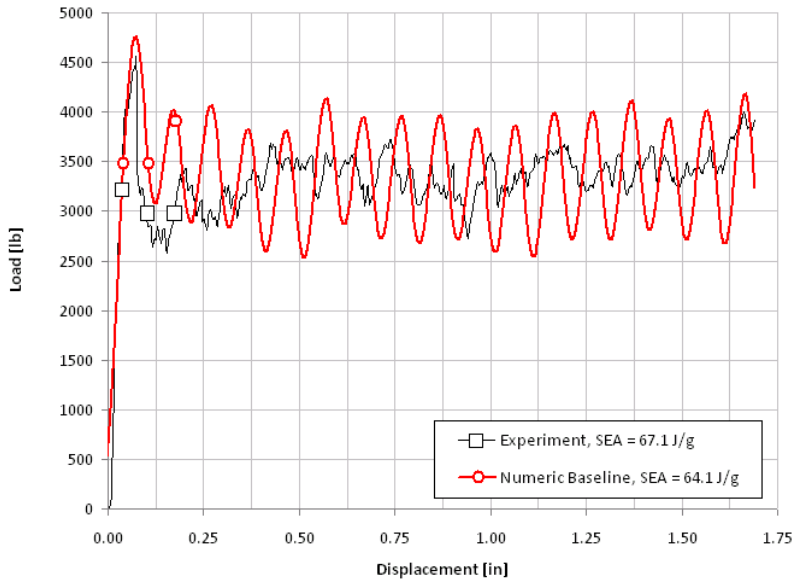

Figure 18. Experimental and Simulation Baseline Crush Curves

The simulation captured all key characteristics of the experimental curve: initial slope, peak load, and average crush load, which, in turn, was used to compare the simulated SEA value to the experimentally measured SEA. The predicted value was 64.12 J/g, compared to the experimental 67.06 J/g, the difference being -4.4%.

The time progression of the simulation also indicates stable crushing (figure 19). Failure advanced in an even and stable fashion, through element deletion at the crashfront. When the first ply in an element failed, the element remained upright and did not exhibit a different morphology. Once all plies had failed, the element was deleted. Elements across the entire crashfront row were deleted simultaneously.

It has been demonstrated that the material model MAT54 can be used to generate a model that closely approximates the crush experiment and captures all the significant features of the corrugated crush coupon experiment.

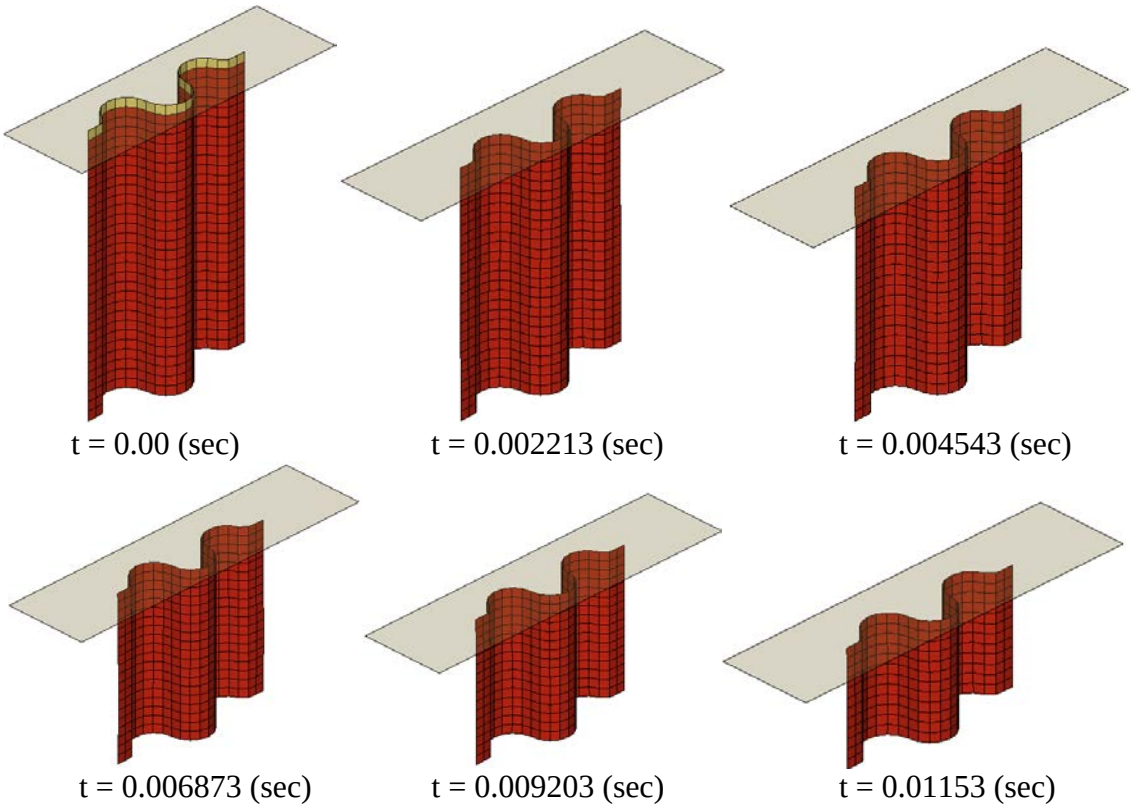

Figure 19. Time Progression of the Baseline Crush Simulation

3.4 PARAMETRIC STUDIES AND RESULTS.

In the first part of the parametric study, the MAT54 material strengths, strains-to-failure, and nonphysical parameters (ALPH, BETA, EFS, FBRT, YCFAC, SOFT, and TFAIL) were investigated. The second part investigated the influence of parameters that are not specific to the material model itself, such as the load velocity, contact type, contact LP curve, mesh size, trigger thickness and geometry, and the SAE postprocessing filter frequency. A summary of the parametric study is given in appendix D.

3.4.1 Parametric Study: MAT54 Material Properties.

This section presents the sensitivity of the baseline simulation to variations in strengths (XT, XC, YT, YC, and SC) and strains to failure (DFAILT, DFAILC, DFAILM, and DFAILS).

Varying longitudinal tensile strength (XT) above or below the baseline value did not affect the outcome of the simulation, except for the extreme cases where the specimen buckles early when XT ≤5 ksi, which would not physically occur. This suggests that fiber tension was not a primary failure driver for this type of simulation with the given specimen geometry-material combination and load condition (compression).

Varying longitudinal compressive strength (XC) had a great effect on the numeric load-displacement curve. Small increments in XC (making it less negative) significantly lowered the average crush load, whereas small decreases in XC (making it more negative) raised the average crush load until a stability threshold was reached and the model became unstable (figure 20). This instability occurred at XC = -275 ksi. The strong dependence of the average crush load on XC suggests that the dominant failure mode occurring in these crush simulations was compressive fiber failure, which is what was expected physically.

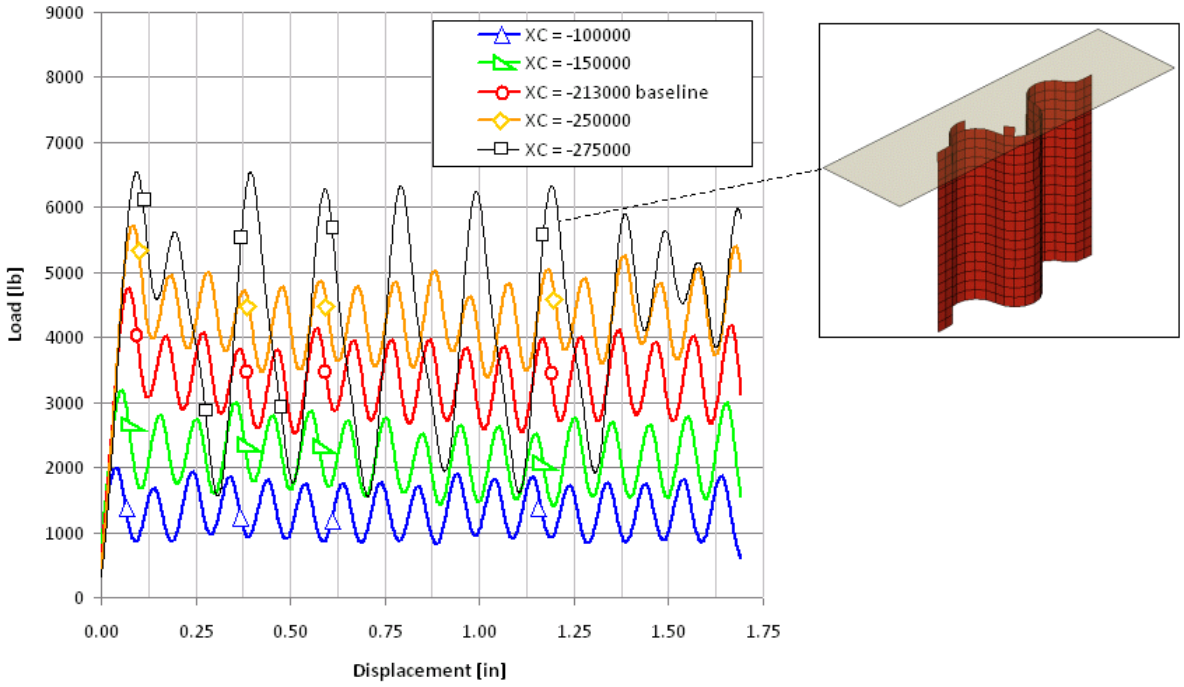

Figure 20. Effect of Varying XC on the Baseline Model

Varying shear strength (SC) had a peculiar influence on the stability of the model. While increasing SC did not affect the results, decreasing SC by even 15% of the experimentally measured value created instabilities in the model, figure 21. Increasingly lower values of SC caused greater instabilities in the crush curve.

MAT54 does not have a failure criterion dedicated to shear failure, but the shear strength term does appear as an interactive term in equations C-4, C-6, and C-7 in appendix C in the tensile fiber, tensile matrix, and compressive matrix failure modes. Decreasing SC increases the contribution of the shear term in this failure criterion, to the point that it causes premature ply and element failure. The results indicate that shear strength is a fundamental parameter for the stability of the simulation. The difference between the baseline (22.4 ksi) and the partially unstable value (19 ksi) is within experimental error, indicating that particular care should be placed in determining the correct experimental value.

Varying the matrix tensile strength (YT) for a range of values from 0 to 300 ksi did not affect the results. The crush curve remained stable, and the average crush load did not change.

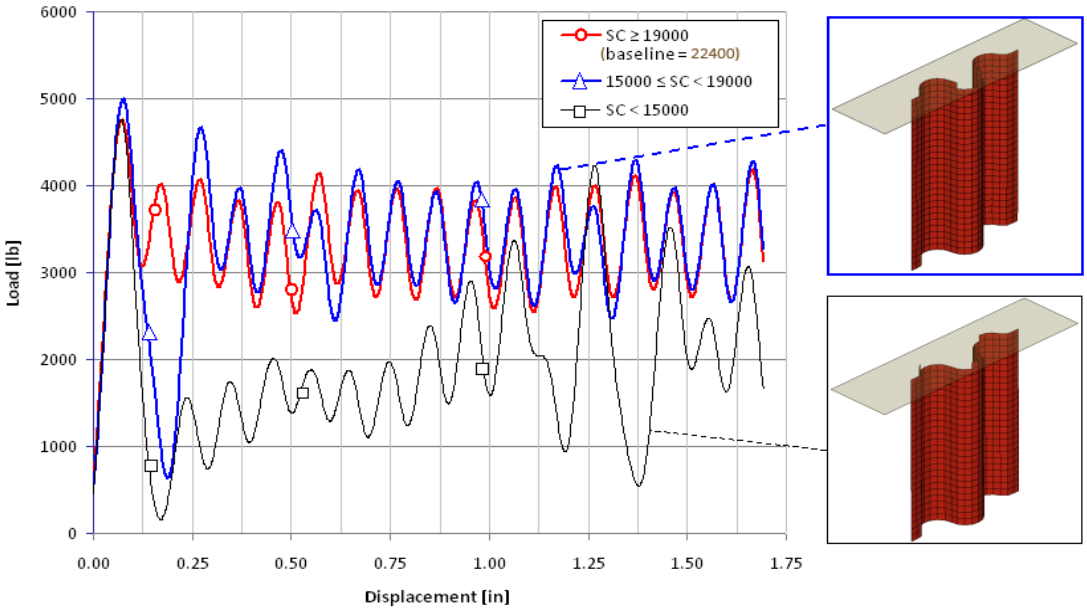

Figure 21. Effect of Varying SC on the Baseline Model

Varying the matrix compressive strength (YC) only changed the results of the crush simulation when especially low values were used, such as 10 ksi, which is less than half the experimentally measured value. This caused slight instabilities. At even lower values of YC, the crush curve dropped significantly (figure 22). This happened as a consequence of the failure mode transitioning from fiber compression to matrix compression by forcibly lowering the matrix compression threshold.

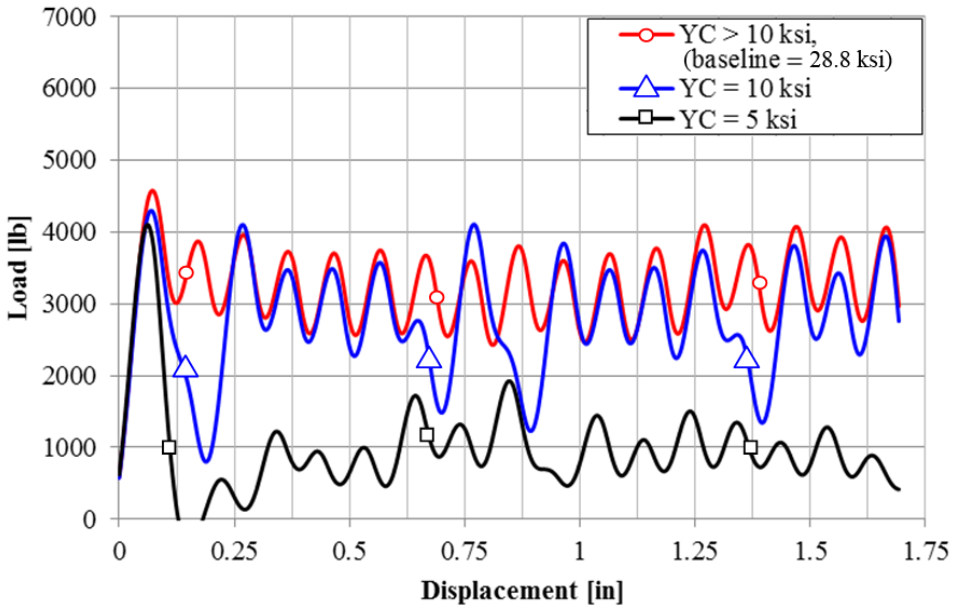

Figure 22. Effect of Varying YC on the Baseline Model

For the fiber tension strain-to-failure (DFAILT), the simulation results remained unchanged from the baseline, which used a value of +0.0174 for values as high as +0.070 and as low as +0.0075. However, when the strain-to-failure was reduced below +0.0075, instabilities began to manifest with nonuniform element failure at both ends of the specimen. For values as low as +0.005, immediate buckling occurred without any stable crushing (figure 23). This suggests that fiber tension failure was not a primary failure mode for the given geometry-material combination, as long as the strain-to-failure was sufficiently large to impede secondary failures.

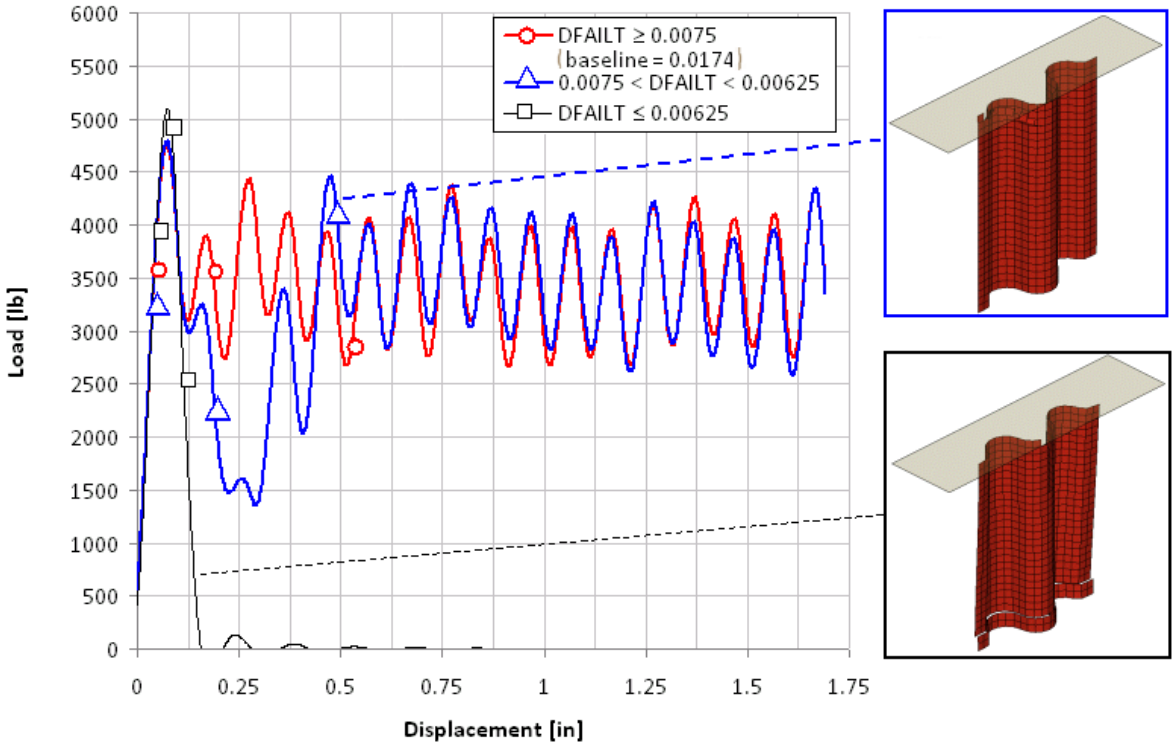

Figure 23. Effect of Varying DFAILT on the Baseline Model

Varying the fiber compressive strain-to-failure DFAILC had a great effect on the model. Small changes in DFAILC directly resulted in great changes in the average crush load, and consequently the SEA. Within a stability range of -0.02 to -0.0081 (baseline value of -0.0116), reducing DFAILC (making it more negative) increased the average crush load, whereas increasing DFAILC (making it less negative) decreased the average crush load (figure 24).

Lowering DFAILC below -0.02 led to nonuniform element deletion at the crashfront, whereas increasing DFAILC up to -0.0081 caused immediate global buckling of the crush coupon (figure 25). Based on these results, compressive strain-to-failure is a primary failure mode for the given specimen geometry-material combination, and therefore, a critical parameter for achieving successful simulation results.

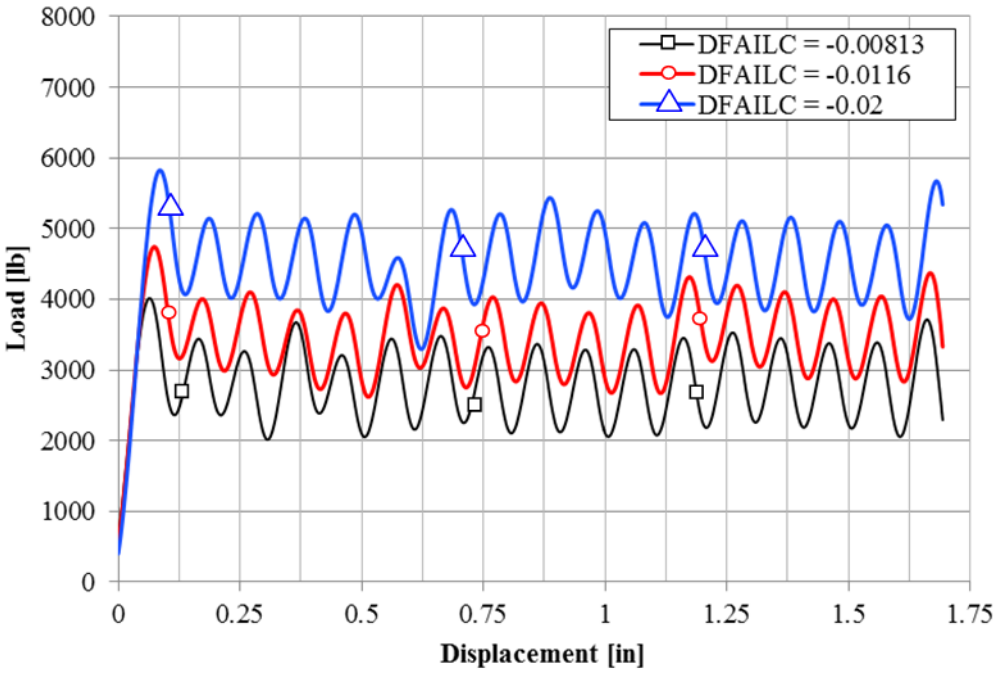

Figure 24. Effect of Varying DFAILC Within a Stable Region of Values

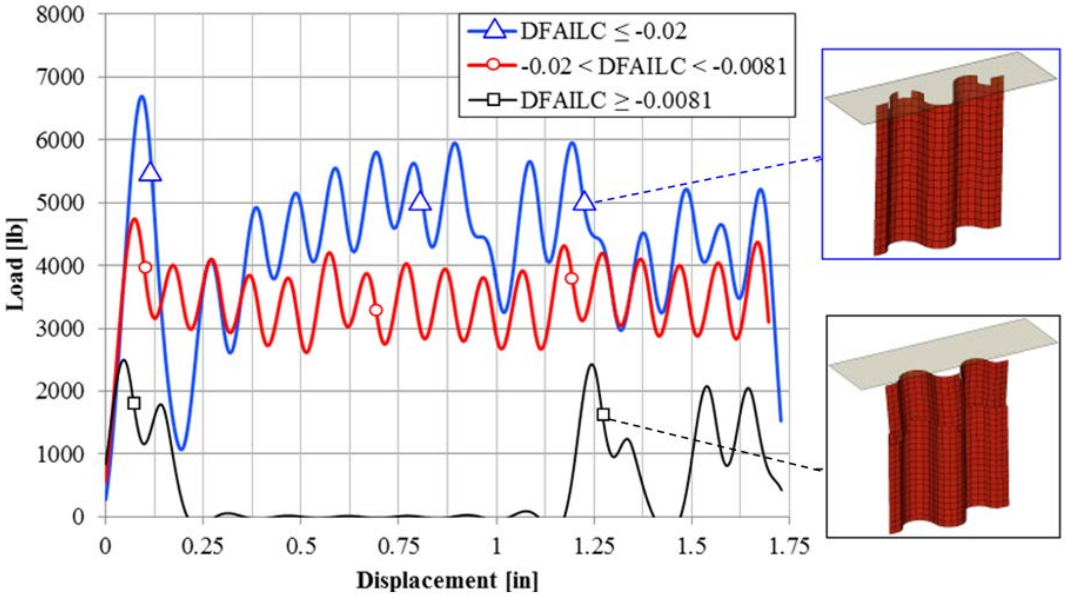

Figure 25. Effect of Varying DFAILC Outside a Stable Region of Values

In the transverse direction, the tension and compressive failure strains are both defined by a single parameter, DFAILM. Since from experiment, the compressive strength of the matrix was greater than its tensile strength (shown in appendix A), it is not feasible to define a single strain-to-failure value for both loading directions. As such, this is a limitation of the MAT54 material

model. For the baseline simulation, DFAILM was set to be the compressive strain-to-failure 0.0240, which automatically imposed a plateau of "virtual plasticity" in tension (figure 15). Adding more plasticity by increasing DFAILM to values as high as 0.100 did not affect the simulation. Decreasing DFAILM beyond the critical value of 0.0165 led to great instabilities, causing nonuniform element deletion at the crashfront and large load fluctuations (figure 26). Setting DFAILM to zero caused severe element distortion, element detachment without deletion, and nonuniform deletion. These findings indicate that DFAILM is a fundamental parameter for the stability of the simulation.

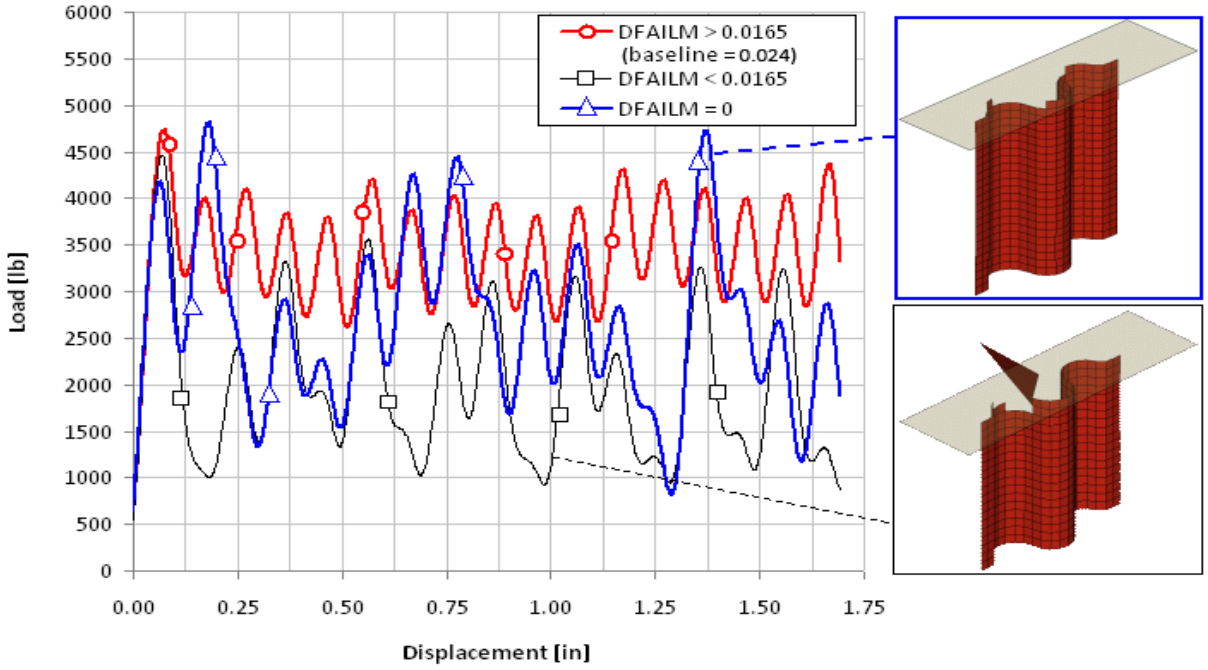

Figure 26. Effect of Varying DFAILM on the Baseline Model

Varying the shear strain-to-failure (DFAILS) had no effect on the simulation, which suggests that either shear is not a dominant failure mechanism for this crush problem or the model is not able to capture shear-related phenomena. Although MAT54 allows element deletion if the strain exceeds DFAILT, DFAILC, or DFAILM, there is no explicit criterion for deletion associated with DFAILS (appendix C).

The EFS parameter is a general failure strain value used as a ply deletion criterion when the effective strain of a ply, given by equation 2, surpasses EFS. Premature ply deletion was obtained when EFS = 0.005; however, deletion occurred away from the crashfront and the corrugated coupon disintegrated within the first several time steps (figure 27). For this type of crash simulation, it is recommended that the experimentally measured failure strains be used for the unidirectional lamina and not the EFS parameter.

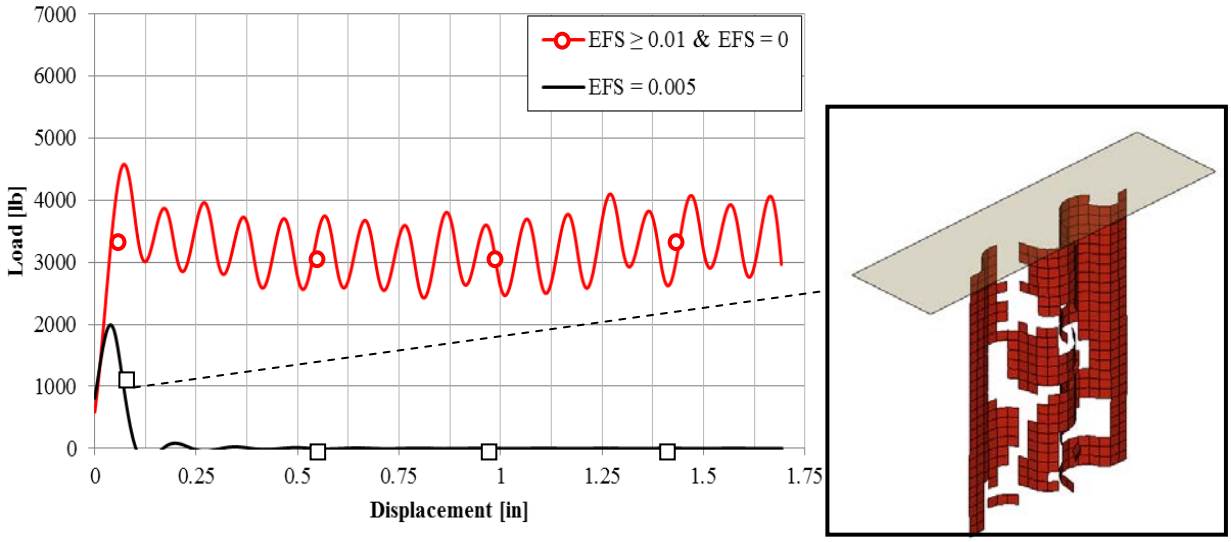

Figure 27. Effect of Using a Small EFS Value on the Baseline Simulation

From these findings, it appears that XC and DFAILC are the dominant parameters leading to element failure and have the strongest influence on simulation results. Other MAT54 material property parameters, such as DFAILM and SC, can have a significant effect on the stability of the model if not properly defined.

3.4.2 Parametric Study: Other MAT54 Parameters.

This section presents the sensitivity of the baseline simulation to variations in MAT54 parameters, which are nonphysical but necessary for the simulation to progress. These parameters either have no significance in the physical world or cannot be measured experimentally and, hence, have to be calibrated by trial and error. These quantities include ALPH, BETA, FBRT, YCFAC, TFAIL, and SOFT.

The ALPH and BETA parameters are shear stress weighing factors that appear in equations C-3 and C-4 in appendix C, respectively. Parametric studies revealed that using any value of ALPH or BETA in the admissible range from 0 to 1 did not influence the baseline simulation in any way, except for the case when ALPH is zero or very close to zero. The independence of the BETA term suggested that shear stress had no effect on fiber failure, which also implied that the failure criterion for tensile fiber failure, give by equation C-4 in appendix C, could either be Hashin (BETA = 1) or maximum stress (BETA = 0) without consequence on the results of the crush simulation. This agreed with the finding that parameters which influence fiber tension failure, XT, and DFAILT did not influence this crush model.

When ALPH was set to zero, crush initiation became unstable, and the first two rows of elements were deleted simultaneously, which caused a significant drop in load after the first load peak followed by stable crushing, as shown in figure 28. When ALPH was set to very small nonzero values, ALPH <1.0E-4, global buckling occurred away from the crashfront (figure 28). The ALPH parameter, which adds the third-order shear term in the elastic shear stress-strain equation,

given by equation C-3 in appendix C, was necessary. However, once it was large enough to allow for the third-order term to take influence, its magnitude did not affect the simulation. Values as high as ALPH = 1 yielded the same results in crush curve and SEA as ALPH = 1.0E-3.

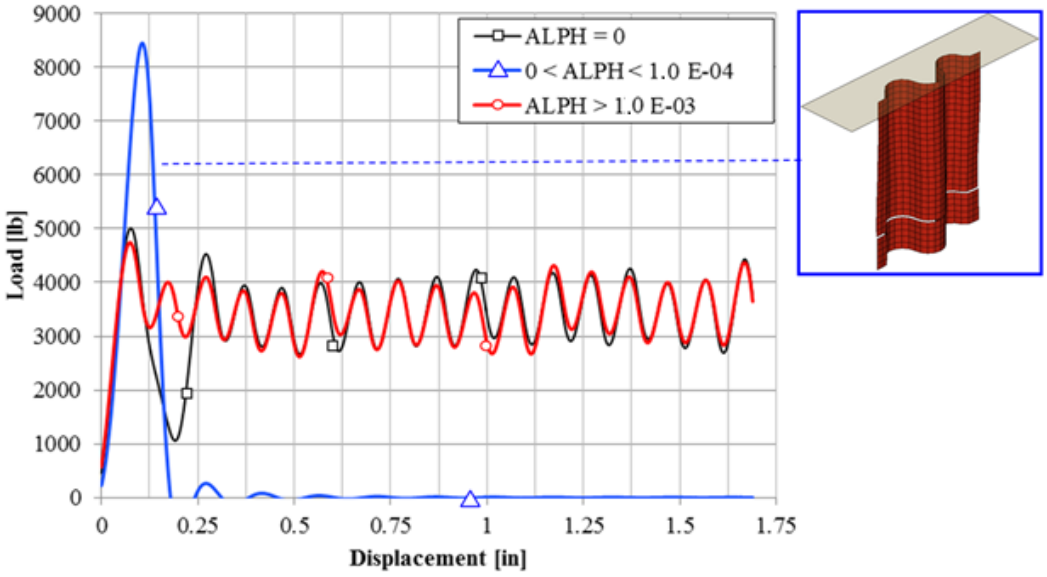

Figure 28. Effect of the Small ALPH Values on the Baseline Model

The strength reduction factors FBRT and YCFAC degrade the tensile and compressive fiber strength of an element after compressive matrix failure has occurred in one of the plies, as dictated by equations 3 and 4. Varying these parameters to the extremes of their admissible ranges yielded negligible change to the baseline simulation, indicating that compressive matrix failure was not a dominating failure mode since no fiber strength degradation was evident.

Varying TFAIL did not affect the simulation, provided its value remained less than the time step of the simulation and larger than zero. When TFAIL was zero, the SOFT parameter automatically became inactive, which is unacceptable for a crash simulation (appendix C), and led to immediate global buckling. When TFAIL was defined to be larger than the simulation time step, all the elements were deleted before being loaded, and the simulation terminated prematurely.

Varying SOFT within the admissible range from 0 to 1 (figure 29) showed that this parameter had a dramatic effect on the simulation, and was the most influential parameter in the entire MAT54 input deck for crush simulations. It alone was capable of dictating whether the simulation was stable or unstable, and it could shift the average crush load above or below the baseline value of 64.12 J/g by at least 30%. Crush curve results are shown in figure 30, where increasing SOFT increased the average crush load and SEA until the model became too stiff and buckled at SOFT = 0.8. Decreasing SOFT lowered the average crush load and SEA indefinitely. Table 2 summarizes these findings.

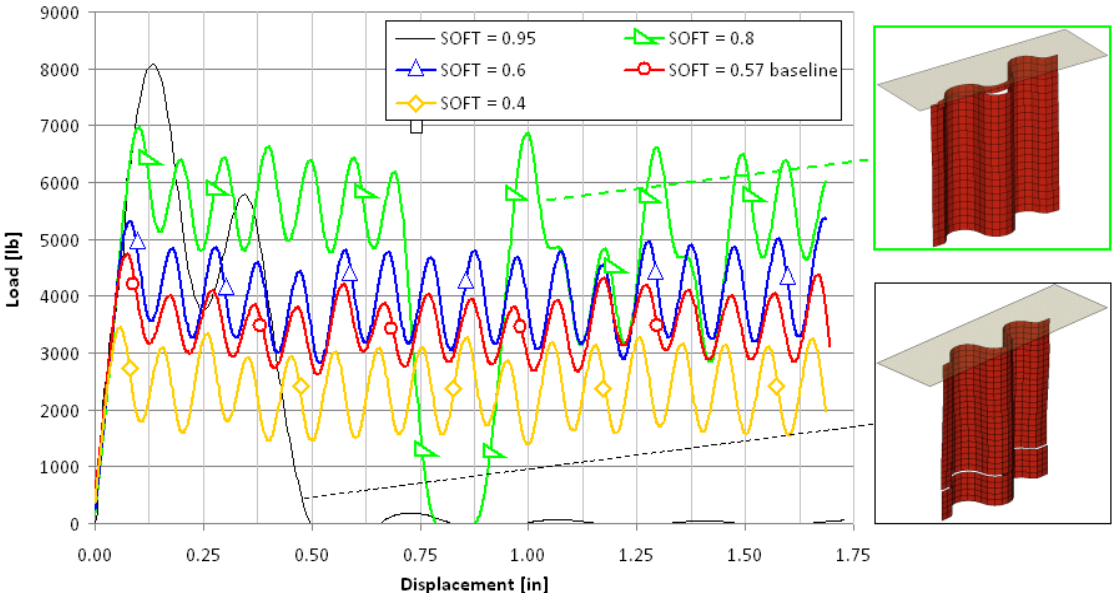

Figure 29. Effect of Varying SOFT on the Baseline Model

Table 2. The SEA Results Obtained by Varying the SOFT Parameter

SOFT	SEA (J/g)	% Change	Failure Mode
0.00	7.71	-88	Global buckling
0.05	2.74	-96	Progressive crush
0.40	48.8	-27	Progressive crush
0.57	64.1	-	Progressive crush
0.60	75.8	+13	Progressive crush
0.80	87.1	+30	Crush + buckling
0.95	8.16	-87	Global buckling
1.00	7.71	-88	Global buckling

Recall that the SOFT parameter is the crashfront parameter that reduces the XT, XC, YT, and YC strengths of the elements at the crashfront. The purpose of the strength reduction is to avoid global buckling that would occur if the peak load was transferred instantaneously upon element deletion from the crashfront to the next row of elements. The SOFT can, therefore, be physically interpreted as a damage zone (comprised of delaminations and cracks) ahead of the crashfront that reduces the pristine strength of the material. Determining the correct SOFT value can only be accomplished through trial and error to match experimental results. As a consequence, this observation concludes that the MAT54 material model is by no means a true predictive tool, since the SOFT parameter needs to be calibrated to the experiment.

3.4.3 Parametric Study: Other Modeling Parameters.

This section presents the sensitivity of the baseline simulation to parameters that are not specific to the material model itself. These parameters include the contact type and LP curve, trigger thickness and geometry, mesh size, load velocity, and the SAE postprocessing filter frequency.

Three alternative contact types were implemented in the crush model: Rigid Nodes to Rigid Body (RN2RB), Eroding Surface to Surface, and Automatic Surface to Surface. Very good results were obtained from the RN2RB contact type. However, the thickness of the trigger row of elements had to be recalibrated to a higher value of 0.052 in. from 0.01 in. to capture the correct initial load peak. Without changing any other parameters but the trigger thickness, the crush curve and SEA results obtained from the RN2RB contact type were nearly identical to using the baseline default Entity contact type, as shown in figure 30.

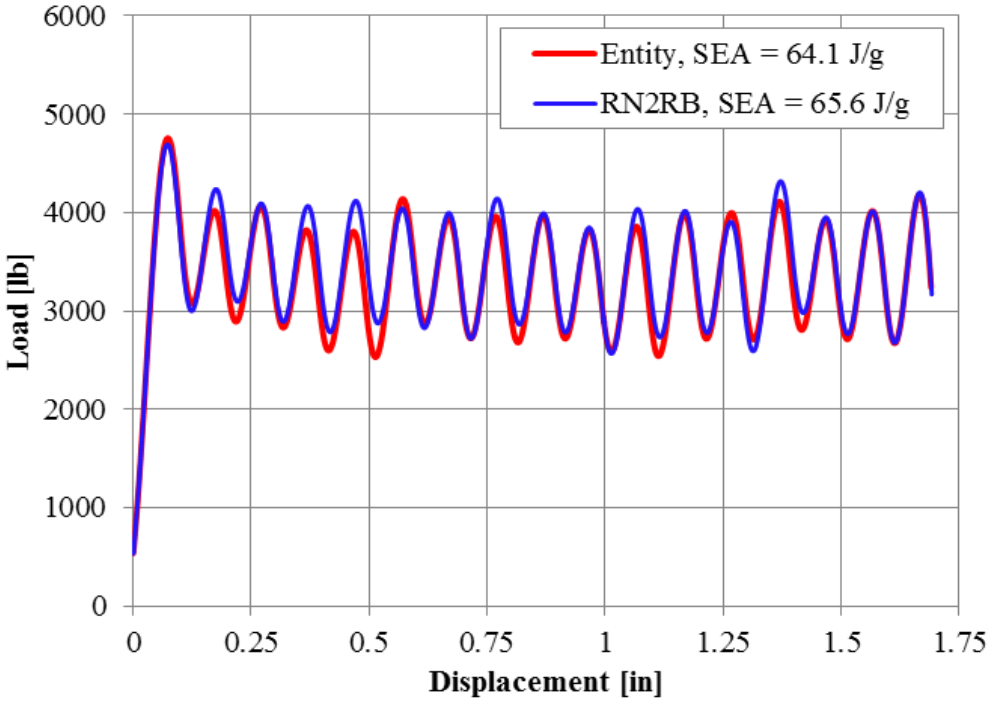

Figure 30. Comparing the RN2RB Contact Type With the Entity Contact Type on the Baseline Model

When a row of elements came into contact with the loading plate while using both Surface-to-Surface contact types, a sharp impulse load was generated and the crashfront row of elements experienced immediate deletion and a return to zero load (figure 31). This loading behavior prevented a stable crush load value from being reached and is, therefore, not compatible with the crush simulation.

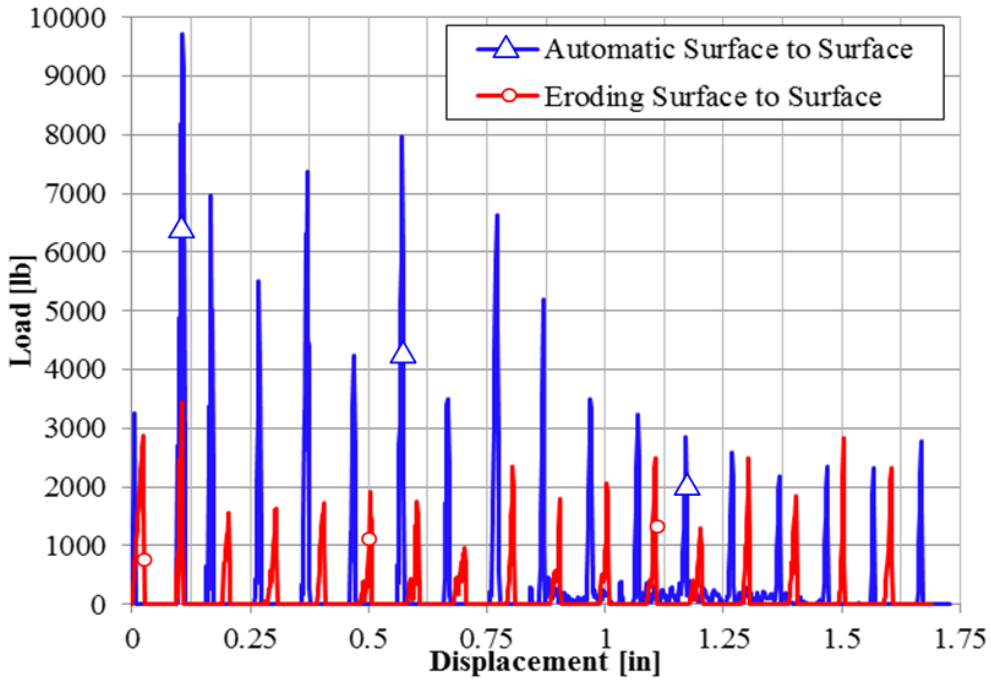

Figure 31. Undesired Crush Curves Generated by Surface to Surface Contact Types

Varying the contact LP curve had a deep effect on the stability of the model, yet there is no way of experimentally determining the correct shape of this curve for the specific material, geometry, and loading combination. The LP curve was defined by trial and error. It has been shown that the piecewise linear (PCWL) baseline LP curve given in figure 16 works well with several coupon-level crush simulations that are similar to the material, geometry, and loading configuration presented in reference 40. Three alternative LP curves were investigated and are shown in figure 32—two PCWL curves with stiffness above and below the baseline and one linear curve with the same final magnitude of the PCWL baseline LP curve. The stiff PCWL curve introduced the load into the coupon more suddenly, while the soft PCWL curve introduced the load more gradually.

It should be expected that using a stiff LP curve would increase the slope of the load-displacement curve (i.e., the load rises faster to its plateau) and increase the reaction forces on the elements at the contact due to the larger reaction loads defined. The opposite should be expected for a soft LP curve. Filtered results showed that the stiff LP curve generated greater initial stiffness than expected but lower peak load and average crush load, while the soft LP curve generated lower initial stiffness but higher peak load and average crush load than the baseline (figure 33). This counterintuitive result was an incompatibility issue of the postprocessing filtering scheme.

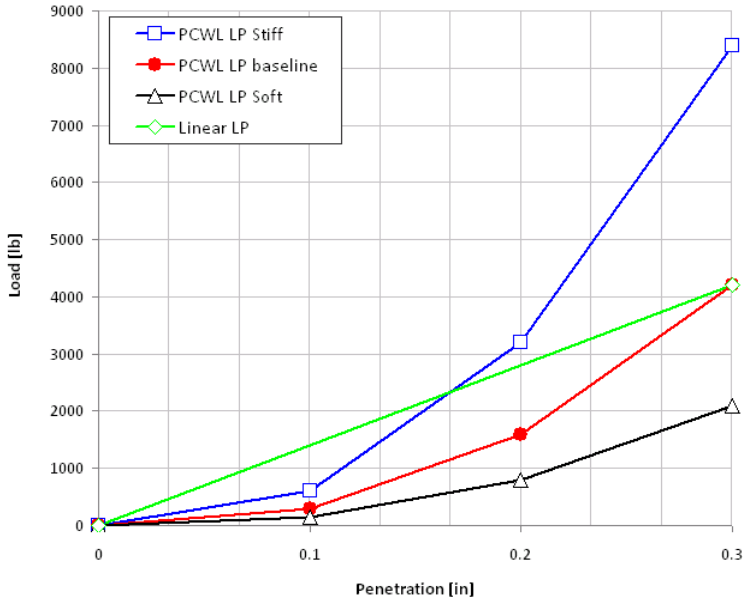

Figure 32. Four LP Curves Investigated

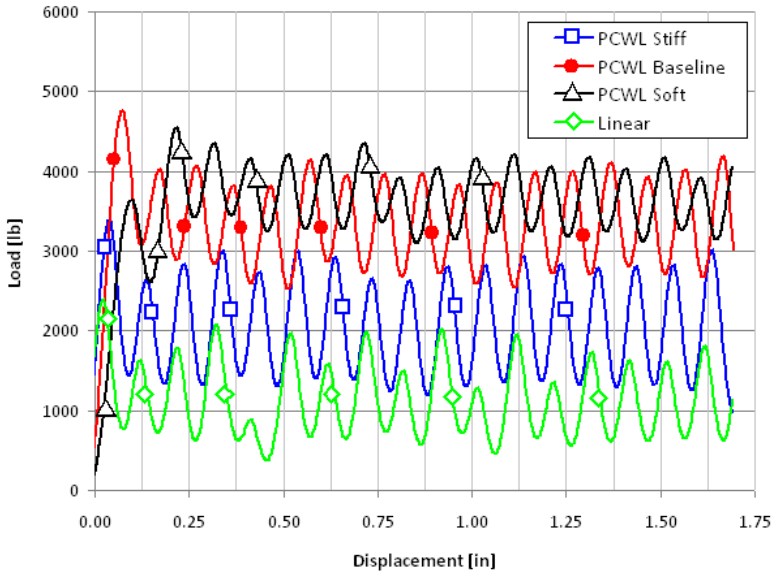

Figure 33. Effect of Varying the Contact LP Curve on the Baseline Model

Considering the raw unfiltered numeric data for the PCWL stiff and PCWL baseline LP curves, shown in figure 34, the stiff LP curve generated higher peak loads than the baseline curve. These high loads led to early element failure and deletion before the loading plate reached the next row of elements, resulting in periods of zero load in between element rows. The zero load regions decreased the average crush load, as calculated with the SAE filter. Therefore, when an aggressive linear LP curve was used (figure 32), the filtered crush curve showed a higher initial stiffness but an even lower average crush load than the stiff PCWL LP curve, as shown in figure 33.

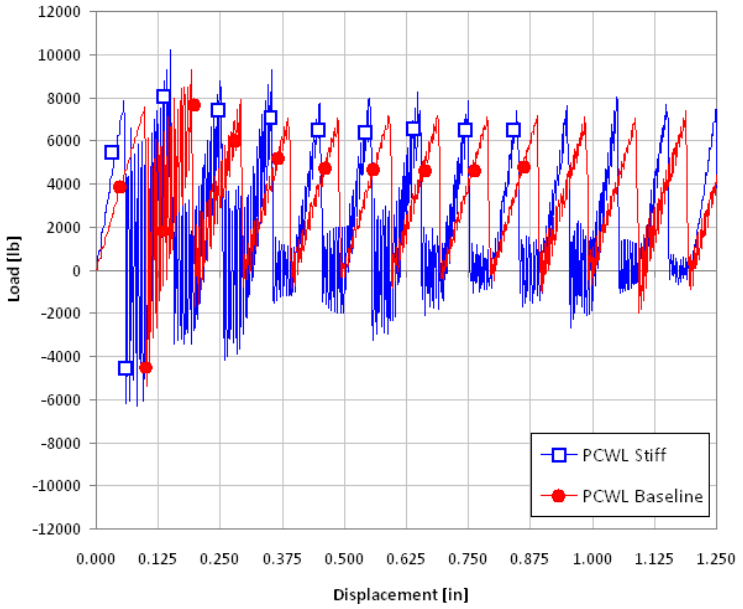

Figure 34. Unfiltered Crush Curves Using the Baseline and the Stiff LP Curves

To observe the effect the LP curve had on the initial stiffness, the initial unfiltered crush load-displacement curves corresponding to the four LP curves are shown in figure 35. The linear LP curve, which had the highest stiffness of the four curves, generated the highest initial stiffness, while the soft PCWL LP curve generated the lowest initial stiffness. The contact LP curve directly influenced the initial slope of the crush load-displacement curve. Careful attention must be paid to the raw data during the filtering process to ensure that the LP curve is not overly stiff, resulting in false filtered data.

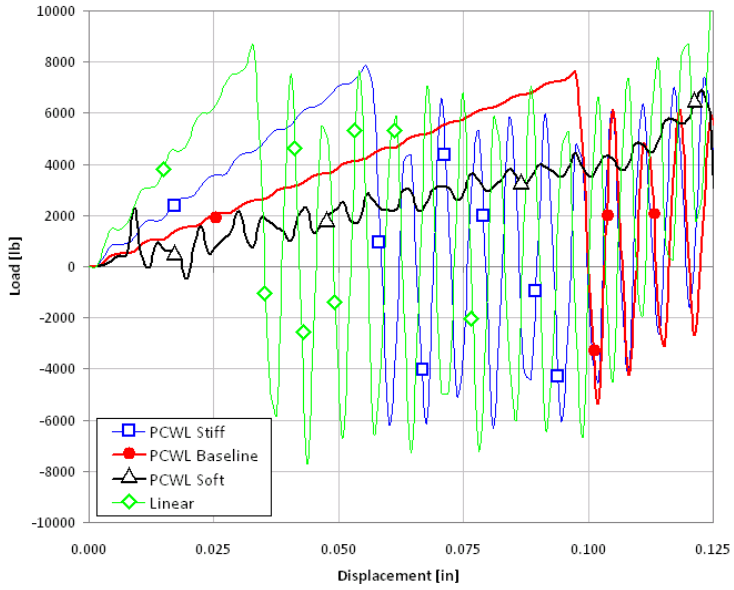

Figure 35. Influence of Varying LP Curves on the Initial Time Steps of the Unfiltered Specimen Crush Load-Displacement Results

The crush trigger directly influenced the initial peak load value and also influenced overall crush stability. The baseline trigger geometry was a single row of elements 0.01 in. thick. Since the trigger was at the contact interface of the loading plate, the choice of contact formulation affected the sensitivity of the simulation results to the trigger thickness. For the Entity contact type, a very thin trigger row of elements (0.01 in.) initiated stable crushing and produced the best results for the crush simulation. Increasing the trigger thickness with the Entity contact type led to random instabilities, as shown in figure 36. Using a trigger thickness larger than the baseline but still relatively thin, such as 0.02 in., led to immediate deletion of both the trigger and second row of elements. This caused a delay in the loading, and there was virtually no initial load peak. Moderate trigger thicknesses, such as 0.04 in., caused uneven element deletion of the second row of elements following the trigger, thus slightly lowering the initial peak. Very high trigger thicknesses, such as 0.06 in., were too stiff and caused global buckling of the crush coupon upon trigger element failure.

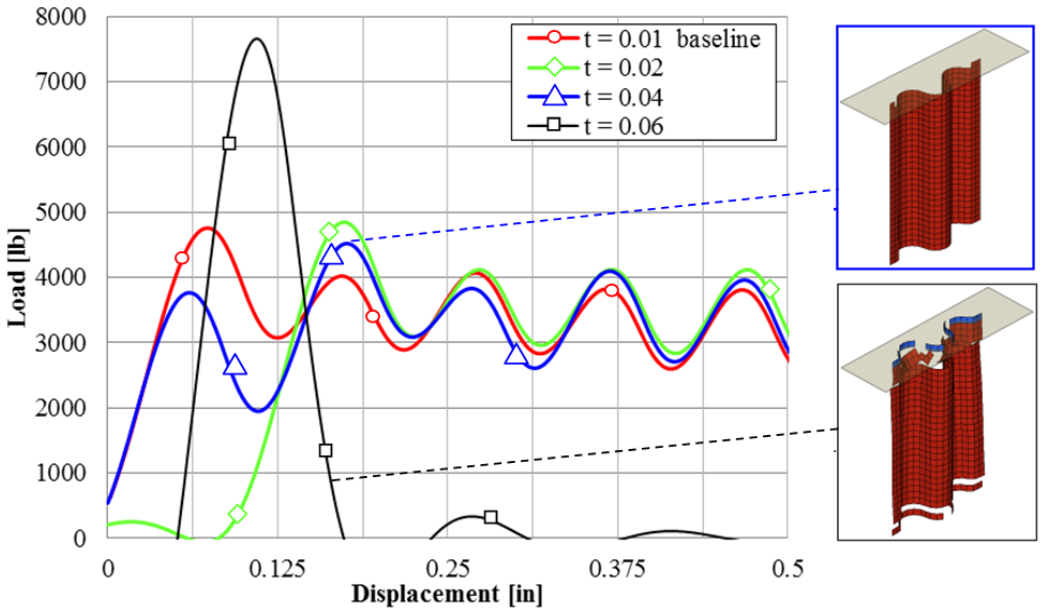

Figure 36. Effect of Varying the Trigger Thickness When Using the Entity Contact Type

Unlike the Entity contact type, the trigger thickness for the RN2RB contact type had a linear effect on the initial load peak and did not lead to random instabilities. Increasing the trigger thickness increased the initial load peak until it was too stiff, and the elements away from the crashfront failed before the trigger elements (figure 37).

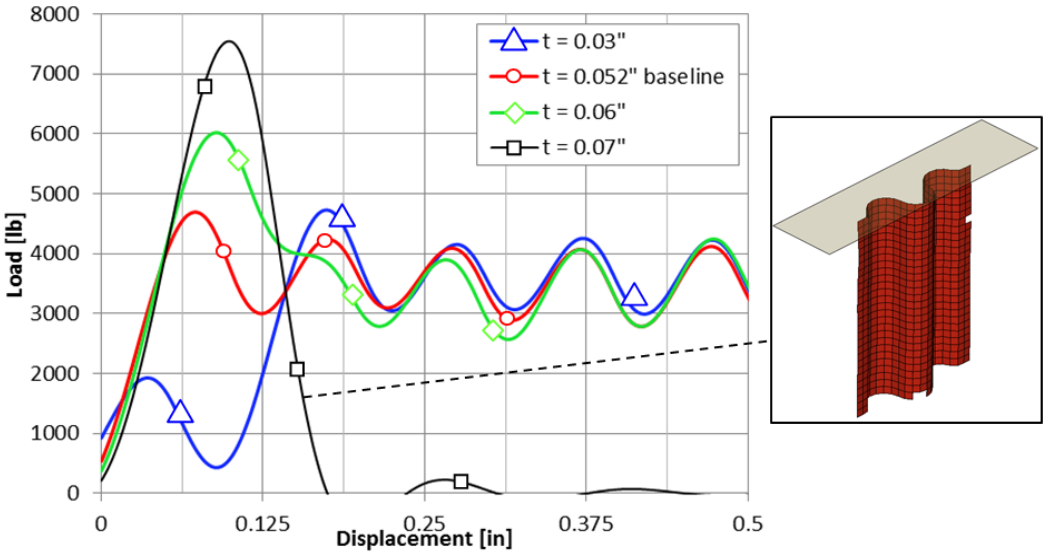

Figure 37. Effect of Varying the Trigger Thickness When Using the RN2RB Contact Type

An alternate trigger geometry was investigated using the Entity contact type. This trigger consisted of a single row of elements with a tapered thickness that varied linearly from 0 to 0.079 in. so it more closely resembled the geometry of the experimental crush trigger. The tapered trigger had a slightly lower load peak than the constant thickness trigger; however, the global response and average crush load were nearly identical (figure 38).

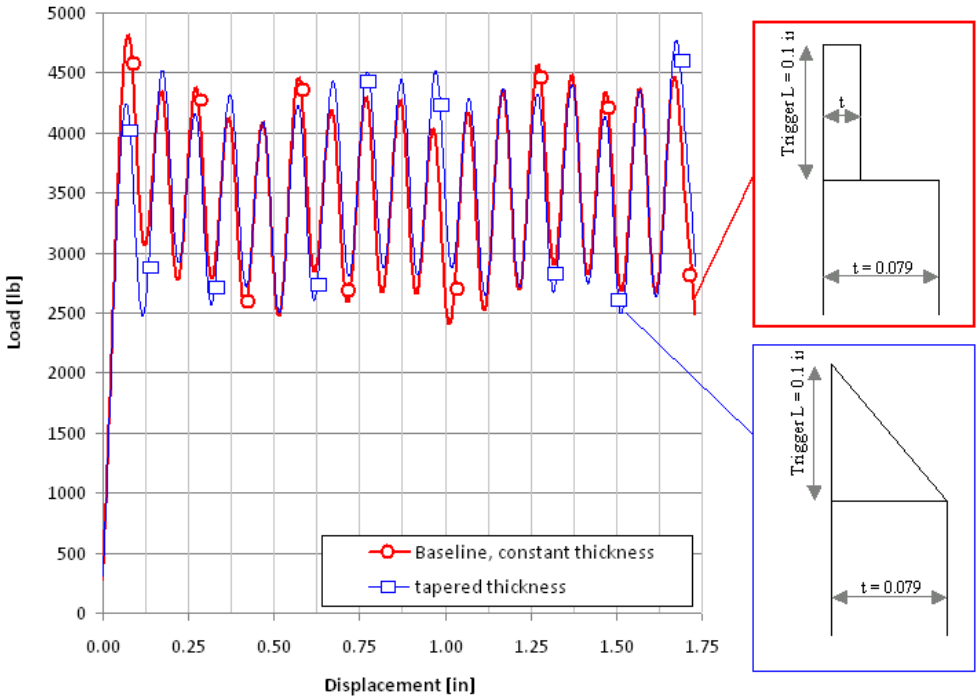

Figure 38. Effect of Using an Alternate Crush Trigger Geometry

The mesh of the crush coupon was varied from the baseline value of 0.1 in. down to 0.05 in. and up to 0.2 in. to study the mesh sensitivity of the crush coupon model. All other parameters were unchanged. The filtered results for the coarse 0.2-in. mesh showed that the initial load and slope were very close to the baseline, but the curve did not achieve a stable crush load (figure 39(a)). Although the coarse mesh produced the same local load peak values as the baseline, the curve oscillated with greater amplitude, reaching zero load between peaks. The zero load regions, also evident in the unfiltered data, were a result of the mesh being too coarse (figure 39(b)), so there was a gap between the failure of one element row and the contact of the following row with the loading plate, similarly to the stiff LP curve case.

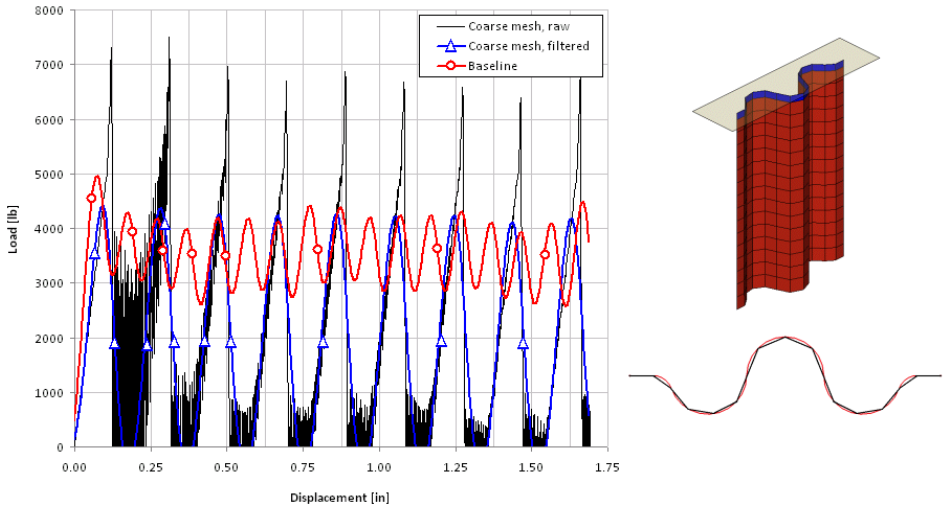

(a) (b)

Figure 39. (a) Effect of Using a Coarse Mesh on Filtered and Unfiltered Load-Displacement Results and (b) Corrugated Model Results

Attempts to calibrate the coarse mesh model (by softening the LP curve or increasing the SOFT parameter), so that acceptable results were obtained, revealed that sustained crushing without zero loading could not be achieved. The coarse mesh size was too coarse to capture the relevant behaviors. This was apparent also when the cross-sectional geometry that the linear shell elements created when coarsely meshed was considered. Since the elements are linear, they cannot curve or bend to conform to a curved geometry. The coarse mesh did not adequately approximate the sinusoid specimen, which is characterized by continuous curvature, as shown in figure 39(b). Quadratic shell elements are currently not available in LS-DYNA [27].

The finer mesh yielded the load-displacement curve shown in figure 40. Without changing any other parameters, the load had a larger initial slope and peak value, followed by instabilities and large oscillations that eventually led to the global buckling of the coupon. By reducing the SOFT parameter from 0.57 to 0.50, the finer-mesh simulation achieved sustained crushing, with only some instability at the beginning of the simulation. Attempts to further stabilize the model by altering the LP curve yielded unstable results. The oscillations for the modified fine-mesh model had a higher frequency as a result of the element rows being doubled, but overall, the finer-mesh model matched the experimental data well.

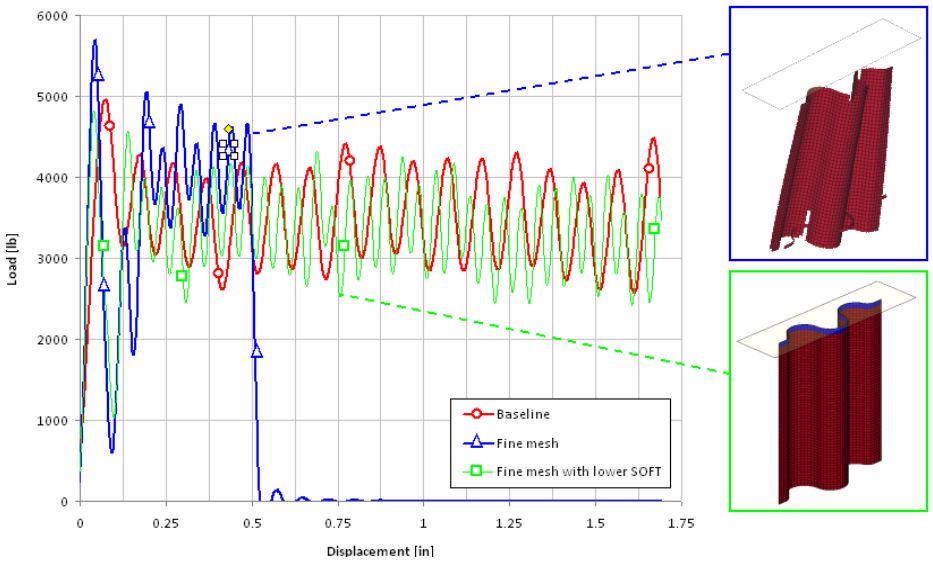

Figure 40. Effect of Using a Fine Mesh on the Baseline Model With and Without a Reduced SOFT Parameter

Although the experimental crush loading rate was 2.0 in./min, simulations were performed using a crush velocity of 150 in./sec due to computational runtime limitations. Crush experiments were conducted at various loading rates to demonstrate the strain rate independence of the SEA in the crush test at these velocities. Results from these experiments are shown in figure 41. Furthermore, since strain rate-dependent material properties are not defined in the material model, the analysis should also show strain rate independence. To verify the validity of this statement, simulations were run at rates of 15 and 1.5 in./sec, which were below any dynamic threshold reported in literature [16 and 29]. Reducing the simulated crush velocity did not significantly change the results (figure 42).

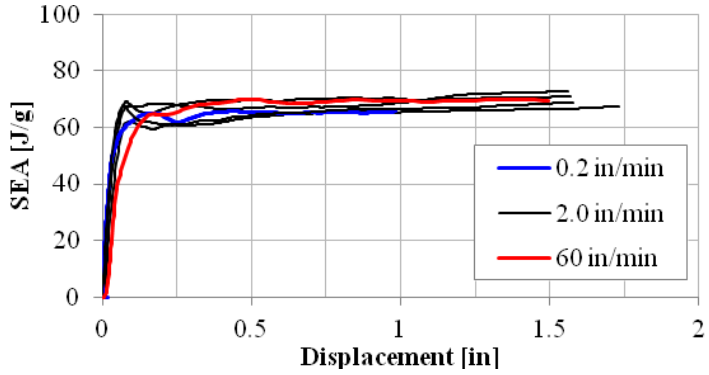

Figure 41. Effect on SEA of Varying the Load Velocity on the Crush Experiment

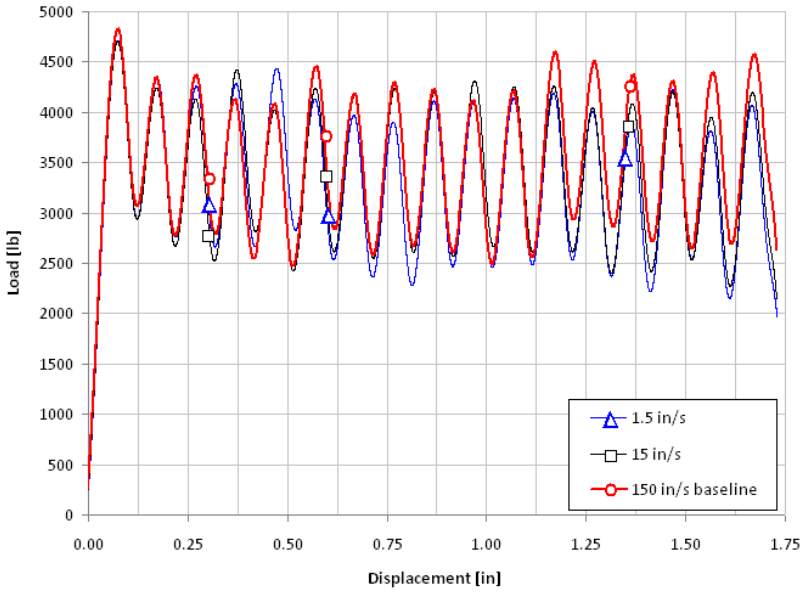

Figure 42. Effect of Varying the Load Velocity on the Baseline Model

The choice of data filter for the postprocessing can significantly change the behavior of the crush curve. Low-pass filters will damp large variations in load; however, it can also mask important physical information, such as the initial slope and peak load. It is desirable to use a frequency that is high enough to capture the initial slope and peak while sufficiently attenuating the load-displacement curve. Typically, the correct low-pass filtering frequency is determined by measuring the duration of the acceleration pulse from accelerometer data recorded during impact. Since this data are not available for the coupon-level test, vehicle impact CFC filters were reviewed to determine the appropriate filter [32]. CFC filters 180 and 1000 were used and compared with the baseline CFC 600 filter (figure 43).

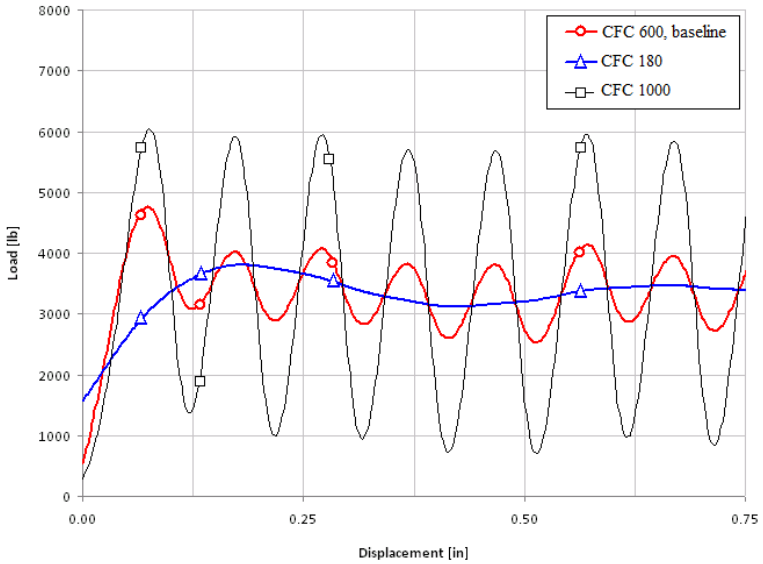

Figure 43. Effect of Varying the SAE Filter Frequency on the Baseline Model

Using the CFC 180 filter caused loss of both the initial slope and peak load, while the CFC 1000 filter retained large load peaks that masked the initial physical peak and stable crush load. The resulting SEA value changed only a few percent, but the overall load-displacement curve lost significance. The filtering also caused a shift of the load-displacement curve to the left, making the initial load in the filtered curve nonzero (figure 43) for all three filter types.

3.5 ANALYTIC DISCUSSION.

A numeric model using the LS-DYNA MAT54 composite material model has successfully been used to simulate the behavior of a corrugated composite coupon undergoing axial crushing in quasi-static loading. A parametric investigation of the MAT54 inputs and other significant modeling parameters was performed, which identified key numeric parameters that are important to this specific modeling approach. The primary MAT54 material parameters, which led to element failure and deletion, have been identified as XC and DFAILC. The SOFT crashfront parameter, however, is the single most influential parameter for determine the success of the simulation. Through trial-and-error calibration, the correct value for SOFT can be identified, which will replicate experimental SEA results. The correct SOFT cannot be determined a priori or by experimental measurement. The DFAILM is particularly critical for the stability of the simulation. The definition of the contact between the loading plate and the coupon, which includes the contact type, the load-penetration curve, and the crush trigger thickness, is also significant to the success and stability of the corrugated crush coupon simulation. In addition, the selection of mesh size and postprocessing filter also adds complexity to the model.

From these findings, it was concluded that this modeling approach is not truly predictive and requires extensive calibration against experimental evidence at the element level (i.e., the corrugated crush specimen). It is important to understand the strengths, weaknesses, and limitations of this modeling approach before venturing into the full-scale simulation.

4. CONCLUSIONS.

This report summarized the results of element-level experiments consisting of the quasi-static crushing of corrugated specimens manufactured with carbon fiber/epoxy prepreg tape. Tests were performed to measure the specific energy absorption and validate the numeric simulation. The corrugated shape is representative of subfloor crashworthy structures used in fixed-wing aircraft and rotorcraft. The corrugated geometry is also appealing from a test perspective since it is self-supporting (i.e., it does not require a stabilizing fixture), it does not feature hoop tensile stress phenomena typical of tubular structures, and it is easy to manufacture. Crush tests showed very stable and progressive crushing associated with large values of energy absorbed.

A detailed explanation of the modeling approach used to simulate the crush test was also included in this report. The finite element model was generated using the commercially available explicit software LS-DYNA. The built-in progressive failure material model MAT54 was successfully used to obtain excellent agreement with the experiment. However, for the model to be considered predictive, it should be based solely on coupon-level material properties obtained from standard lamina-level material tests. Several modeling parameters, which have no corresponding physical meaning or cannot otherwise be measured experimentally, have a strong

influence on the success of the simulation. These parameters need to be calibrated by trial and error to match the experimental results of the structural element crush tests of the corrugated specimen. Therefore, the modeling approach cannot be considered to be truly predictive at this level of structural complexity.

The implications are that the element-level tests (e.g., the crushing of an energy-absorbing component, such as the corrugated specimen) should be used for model calibration and not validation, within the certification strategy by analysis supported by test evidence. Once the model is calibrated at this level, the analysis model can be used at higher levels of complexity to predict the crash response of subcomponents, components, and full-scale test articles.

5. REFERENCES.

1. Composite Materials Handbook (CMH-17) Volume 3, Chapter 16, Rev. G.

2. Cronkhite, J.D., Chung, Y.T., and Bark, L.W., "Crashworthy Composite Structures," USAAVSCOM TR-87-D-10, U.S. Army, December 1987.

3. Desjardins, S., Zimmerman, R.E., and Merritt, N.A., "Aircraft Crash Survival Design Guide," Volume III: Aircraft Structural Crash Resistance, U.S. Army Aviation Systems Command, USAAVSCOM TR-89-D-22C, December 1989.

4. Cronkhite, J.D., Haas, T.J., Winter, R., and Singley, G.T., "Investigation of the Crash Impact Characteristics of Composite Airframe Structures," *34th AHS Annual Forum*, pp. 52-63, May 1978.

5. Jackson, K.E., Fasanella, E.L., Boitnott, R.L., McEntire, J., and Lewis, A., "Occupant Responses in a Full-Scale Crash Test of a Sikorsky ACAP Helicopter," NASA TM-2002-211733, June 2002.

6. Jackson, K.E., Fasanella, E.L., Boitnott, R.L., and Lyle, K.H., "Full-Scale Crash Test and Finite Element Simulation of a Composite Prototype Helicopter," NASA TP-2003-212641, August 2003.

7. Kay, B., "SARAP Virtual Prototype and Validation Program Overview," *AHS Technical Specialist Meeting on Rotorcraft Structures and Survivability*, October 2005.

8. Carden, H.D. and Kellas, S., "Energy-Absorbing Beam Design for Composite Aircraft Subfloors," *Proceedings of the 34th AIAA Structures, Structural Dynamics, and Materials Conference*, La Jolla, California, April 19-21, 1993.

9. Johnson, A. and Kohlgruber, D., "Design and Performance of Energy Abosorbing Subfloor Structures in Aerospace Applications," *IMechE Seminar S672*, London, England, May 2000.

10. McCarthy, M.A. and Wiggenraad, J.F.M., "Numerical Investigation of a Crash Test of a Composite Helicopter Subfloor Structure," *Composite Structures*, Vol. 51, pp. 345-359, 2001.

11. Wiggenraad, J.F.M., "Crashworthiness Research at NLR: 1990-2003," NLR TP-2003-217, June 2003.

12. Ubels, L.C. and Wiggenraad, J.F.M., "Increasing the Survivability of Helicopter Accidents Over Water," NLR-TP-2002-110, February 2002.

13. San Vicente, J.L., Beltrán, F., and Martínez, F., "Simulation of Impact on Composite Fuselage Structures," European Congress on Computational Methods in Applied Sciences and Engineering, ECCOMAS 2000, Barcelona, Spain, September 2000.

14. McCarthy, M.A., Harte, G.A., Wiggenraad, J.F.M., Michielsen, A.L.P.J., Kohlgrueber, D., and Kamoulakos, A., "Finite Element Modeling of Crash Response of Composite Aerospace Sub-Floor Structures," *Computational Mechanics*, Vol. 26, pp. 250-258, 2000.

15. Jones, L.E. and Carden, H.D., "Evaluation of Energy Absorption of New Concepts of Aircraft Composite Subfloor Intersections," NASA TP-2951, November 1989.

16. Bannerman, D.C. and Kindervater, C.M., "Crashworthiness Investigation of Composite Aircraft Subfloor Beam Sections," *Structural Impact and Crashworthiness*, Vol. 2 Conference Papers—Elsevier, London, England, 1984.

17. Jackson, K.E., "Energy Absorption of Composite Materials and Structures," *Proceedings of the 49th MIL-HDBK-17 Coordination Meeting—Crashworthiness Working Group*, Santa Monica, California, December 2005.

18. Savage, G., "Development of Penetration Resistance in the Survival Cell of a Formula 1 Racing Car," *Engineering Failure Analysis*, Vol. 17, pp. 116-127, 2010.

19. Savage, G., Bomphray, I., and Oxley, M., "Exploiting the Fracture Properties of Carbon Fibre Composites to Design Lightweight Energy Absorbing Structures," *Engineering Failure Analysis*, Vol. 11, pp. 677-694, 2004.

20. Feraboli, P., Norris, C., and McLarty, D., "Design and Certification of a Composite Thin-Walled Structure for Energy Absorption," *International Journal of Vehicle Design*, Vol. 44, No. 3-4, pp. 15-36, 2007.

21. Jeryan, R., "Energy Management Working Group Activities," *Proceedings of the 48th MIL-HDBK-17 Coordination Meeting—Crashworthiness Working Group*, Charlotte, North Carolina, March 2005.

22. Nailadi, C., "A Summary of the ACC Tube Testing Program," *Proceedings of the 49th MIL-HDBK-17 Coordination Meeting—Crashworthiness Working Group*, Santa Monica, California, December 2005.

23. Browne, A.L., "Automotive Composites Consortium Generic Tube Crush Program: Dynamic Crush Tests of Resin Transfer Molded Tubes," *Proceedings of the 13th ASC Annual Technical Conference*, Baltimore, Maryland, September 1998.

24. Browne, A., Johnson, N., and Botkin, M., "Dynamic Crush Response of RTM Crash Boxes," *ASC 24th Technical Conference*, Memphis, Tennessee, September 2008.

25. Hanagud, S., Craig, I., Sriram, P., and Zhou, W., "Energy Absorption Behaviour of Graphite Epoxy Composite Sine Webs," *Journal of Composite Materials*, Vol. 23, No. 5, pp. 448-459, 1989.

26. Feraboli, P., "Development of a Corrugated Test Specimen for Composite Materials Energy Absorption," *Journal of Composite Materials*, Vol. 42, No. 3, pp. 229-256, 2008.

27. Feraboli, P., "Development of a Modified Flat Plate Test and Fixture Specimen for Composite Materials Crush Energy Absorption," *Journal of Composite Materials*, Vol. 43, No. 19, pp. 1967-1990, 2009.

28. Carruthers, J.J., Kettle, A.P., and Robinson, A.M., "Energy Absorption Capability and Crashworthiness of Composite Material Structures: A Review," *Applied Mechanics Reviews*, No. 51, pp. 635-649, 1998.

29. Johnson, A., "Determination of Composite Energy Absorption Properties," *Proceedings of the 50th MIL-HDBK-17 Coordination Meeting—Crashworthiness Working Group*, Chicago, Illinois, July 2006.

30. Hinton, M.J., Kaddour, A.S., and Soden, P.D., "A Comparison of the Predictive Capabilities of Current Failure Theories for Composite Laminates, Judged Against Experimental Evidence," *Composites Science and Technology*, Vol. 62, No. 12-13, pp. 1725-1797, 2002.

31. Xiao, X., "Modeling Energy Absorption With a Damage Mechanics-Based Composite Material Model," *Journal of Composite Materials*, Vol. 43, No. 5, pp. 427-444, 2009.

32. "Proceedings of the CMH-17 (MIL-HDBK-17) Crashworthiness Working Group Numerical Round Robin," Costa Mesa, California, July 2010.

33. Hallquist, J.O., "LS-DYNA Theoretical Manual," Livermore Software Technology Corporation, 2005.

34. Tho, C., "BA609 Bird Strike Simulation for Design Support Using LS-DYNA," *Proceedings of the American Helicopter Society Technical Specialist's Meeting on Rotorcraft Structures and Survivability*, Williamsburg, Virginia, October 2005.

35. Gabrys, J., Schatz, J., Carney, K., Melis, M., Fasanella, E., and Lyle, K., "The Use of LS-DYNA in the Columbia Accident Investigation and Return to Flight Activities," *Proceedings of the 8th International LS-DYNA Users Conference*, Detroit, Michigan, May 2004.

36. Carney, K.S., Lawrence, C., and Carney, D.V., "Aircraft Engine Blade-Out Dynamics," *Proceedings of the 7th International LS-DYNA Users Conference*, Detroit, Michigan, May 2002.

37. Simmons, J., Erlich, D., and Shockey, D., "Explicit Finite Element Modeling of Multilayer Composite Fabric for Gas Turbine Engine Containment Systems, Part 3: Model Development and Simulation of Experiments," FAA report DOT/FAA/AR-04/40,P3, November 2004.

38. Gomuc, R., "Explicit Finite Element Modeling of Multilayer Composite Fabric for Gas Turbine Engine Containment Systems, Part 4: Model Simulation for Ballistic Tests, Engine Fan Blade-Out, and Generic Engine," FAA report DOT/FAA/AR-04/40,P4, November 2004.

39. Jackson, K.E. and Fasanella, E.L., "Development of an LS-DYNA Model of an ATR42-300 Aircraft for Crash Simulation," *Proceedings of the 8th International LS-DYNA Users Conference*, Detroit, Michigan, May 2004.

40. Feraboli, P., Deleo, F., Wade, B., Rassaian, M., Higgins, M., Byar, A., Reggiani, M., Bonfatti, A., DeOto, L., and Masini, A., "Predictive Modeling of an Energy-Absorbing Sandwich Structural Concept Using the Building Block Approach," *Composites Part A*, Vol. 41, No. 6, pp. 774-786, 2010.

41. Fasanella, E.L. and Jackson, K.E., "Best Practices for Crash Modeling Simulation," NASA TM-2002-211944, ARL-TR-2849, October 2002.

42. Chang, F.K. and Chang, K.Y., "A Progressive Damage Model for Laminated Composites Containing Stress Concentration," *Journal of Composite Materials*, Vol. 21, pp. 834-855, 1987.

APPENDIX A—MATERIAL PROPERTIES OF T700/2510 UNIDIRECTIONAL TAPE
[reference CMH-17]

Property	Symbol	LS-DYNA Parameter	Experimental Value
Density	ρ	RO	0.055 lb/in^3
Modulus in 1-direction	E_1	EA	18.4 Msi
Modulus in 2-direction	E_2	EB	1.22 Msi
Shear modulus	G_{12}	GAB	0.61 Msi
Major Poisson's ratio	ν_{12}	-	0.309
Minor Poisson's ratio	ν_{21}	PRBA	0.02049
Strength in 1-direction, tension	F_1^{tu}	XT	319 ksi
Strength in 2-direction, tension	F_2^{tu}	YT	7.09 ksi
Strength in 1-direction, compression	F_1^{cu}	XC	213 ksi
Strength in 2-direction, compression	F_2^{cu}	YC	28.8 ksi
Shear strength	F_{12}^{su}	SC	22.4 ksi
Strain-to-failure in 1-direction, tension	-	DFAILT	0.0174
Strain-to-failure in 1-direction, compression	-	DFAILC	-0.0116
Strain-to-failure in 2-direction, tension	-	DFAILM	0.006
Strain-to-failure in 2-direction, compression	-		-0.024
Strain-to-failure in the 1-2 direction, shear	-	DFAILS	3%-5%

APPENDIX B—MAT54 PARAMETER DEFINITIONS

Table B-1. Active MAT54 Parameter Definitions

Variable	Definition
MID	Material ID number used by LS-DYNA to assign materials to elements
RO	Density, ρ, of material, mass per unit volume
EA	$E_{1,}$ Young's modulus in longitudinal direction
EB	$E_{2,}$ Young's modulus in transverse direction
PRBA	$v_{21,}$ Minor Poisson's ratio
GAB	$G_{12,}$ Shear modulus
GBC	$G_{23,}$ Shear modulus
GCA	$G_{31,}$ Shear modulus
AOPT MANGLE <V1 V2 V3>	These 5 parameters are used to define the local 1-2-3 coordinate system of the material relative to the global x-y-z coordinate system.
DFAILT	Strain-to-failure for fiber tension
DFAILC	Strain-to-failure for fiber compression
DFAILM	Strain-to-failure for matrix tension and compression
DFAILS	Strain-to-failure for shear
EFS	Effective failure strain
TFAIL	Minimum time step size criteria for element deletion
ALPH	Nonlinear term in the elastic shear stress-strain equation
SOFT	Softening factor for crashfront elements experiencing crush loading
FBRT	Softening factor for fiber tensile strength after matrix failure
YCFAC	Softening factor for fiber compressive strength after matrix failure
BETA	Shear term weighing factor in tensile fiber failure mode equation
XC	F_1^{cu}, Longitudinal compressive strength
XT	F_1^{tu}, Longitudinal tensile strength
YC	F_2^{cu}, Transverse compressive strength
YT	F_2^{tu}, Transverse tensile strength
SC	F_{12}^{tu}, Shear strength
CRIT	Chosen failure criterion: MAT54 Chang-Chang, MAT55 Tsai-Wu

APPENDIX C—LS-DYNA THEORY MANUAL FOR MATERIAL MODEL MAT54

The MAT54 material model uses the MAT22 stress-strain equations in the elastic region, therefore the appropriate portion from the LS-DYNA Theory Manual for MAT22 is presented here in addition to the entire section of the LS-DYNA Theory Manual for the MAT54 material model.

Material Model 22: Chang-Chang Composite Failure Model

In plane stress, the strain is given in terms of the stress as

$$\varepsilon_1 = \frac{1}{E_1}(\sigma_1 - \nu_{12}\sigma_2) \tag{C-1}$$

$$\varepsilon_2 = \frac{1}{E_2}(\sigma_2 - \nu_{21}\sigma_1) \tag{C-2}$$

$$2\varepsilon_{12} = \frac{1}{G_{12}}\tau_{12} + \alpha\tau_{12}^{\ 3} \tag{C-3}$$

The third equation defines the nonlinear shear stress parameter α.

Material Models 54 and 55: Enhanced Composite Damage Model

These models are very close in their formulations. Material 54 uses Chang matrix failure criterion (as Material 22), and material 55 uses the Tsai-Wu criterion for matrix failure.

Arbitrary orthotropic materials, e.g., unidirectional layers in composite shell structures can be defined. Optionally, various types of failure can be specified following either the suggestions of Chang and Chang [C-11] or Tsai and Wu [C-2]. In addition special measures are taken for failure under compression. See Matzenmiller and Schweizerhof [C-3]. This model is only valid for thin shell elements.

The Chang/Chang criteria is given as follows:

for the tensile fiber mode

$$\sigma_{aa} > 0 \text{ then } e_f^2 = \left(\frac{\sigma_{aa}}{X_t}\right)^2 + \beta\left(\frac{\sigma_{aa}}{S_c}\right) - 1 \begin{cases} \geq 0 & \textit{failed} \\ < 0 & \textit{elastic} \end{cases} \tag{C-4}$$

Upon failure: $E_a = E_b = G_{ab} = \nu_{ba} = \nu_{ab} = 0$

for the compressive fiber mode,

$$\sigma_{aa} > 0 \text{ then } e_c^2 = \left(\frac{\sigma_{aa}}{X_c}\right)^2 - 1 \begin{cases} \geq 0 \text{ failed} \\ < 0 \text{ elastic} \end{cases} \tag{C-5}$$

Upon failure: $E_a = \nu_{ba} = \nu_{ab} = 0$

for the tensile matrix mode,

$$\sigma_{bb} > 0 \text{ then } e_m^2 = \left(\frac{\sigma_{bb}}{Y_t}\right)^2 + \left(\frac{\sigma_{ab}}{S_c}\right)^2 - 1 \begin{cases} \geq 0 \text{ failed} \\ < 0 \text{ elastic} \end{cases} \tag{C-6}$$

Upon failure: $E_b = \nu_{ba} = G_{ab} = 0$

and for the compressive matrix mode,

$$\sigma_{bb} < 0 \text{ then } e_d^2 = \left(\frac{\sigma_{bb}}{2S_c}\right)^2 + \left[\left(\frac{Y_c}{2S_c}\right)^2 - 1\right]\frac{\sigma_{bb}}{Y_c} + \left(\frac{\sigma_{ab}}{S_c}\right)^2 - 1 \begin{cases} \geq 0 \text{ failed} \\ < 0 \text{ elastic} \end{cases} \tag{C-7}$$

Upon failure: $E_b = \nu_{ba} = \nu_{ab} = 0 = G_{ab} = 0$
$X_c = 2Y_c$ *for 50% fiber volume*

For $\beta = 1$ we get the original Hashin [c4] in the tensile fiber mode.

For $\beta = 0$, we get the maximum stress criterion which is found to compare better to experiments.

Failure can occur in any of four different ways:

1. If DFAILT is zero, failure occurs if the Chang/Chang failure criterion is satisfied in the tensile fiber mode.

2. If DFAILT is greater than zero, failure occurs if the tensile fiber strain is greater than DFAILT or less than DFAILC.

3. If EFS is greater than zero, failure occurs if the effective strain is greater than EFS.

4. If TFAIL is greater than zero, failure occurs according to the element time step as described in the definition of TFAIL.

When failure has occurred in all the composite layers (through-thickness integration points), the element is deleted. Elements which share nodes with the deleted element become “crashfront” elements and can have their strengths reduced by using the SOFT parameter with TFAIL greater than zero.

Information about the status in each layer (integration point) and element can be plotted using additional integration point variables. The number of additional integration point variables for shells written to the LS-DYNA database is input by the *DATABASE_BINARY definition as variable NEIPS. For Models 54 and 55 these additional variables are tabulated below (*i* = shell integration point):

History Variable	Description	Value	LS-PREPOST History Variable
1. *ef(i)*	*tensile fiber mode*	*1 – elastic* *0 – failed*	*1*
2. *ec(i)*	*compressive fiber mode*		*2*
3. *em(i)*	*tensile matrix mode*		*3*
4. *ed(i)*	*compressive matrix mode*		*4*
5. *efail*	*max[ef(ip)]*		*5*
6. *dam*	*damage parameter*	*-1 – element intact* *10^{-8} – element in crashfront* *+1 – element failed*	*6*

The following components, defined by the sum of failure indicators over all through-thickness integration points, are stored as element component 7 instead of the effective plastic strain.

Description	Integration point
$\frac{1}{nip}\sum_{i=1}^{nip} ef(i)$	*1*
$\frac{1}{nip}\sum_{i=1}^{nip} ec(i)$	*2*
$\frac{1}{nip}\sum_{i=1}^{nip} em(i)$	*3*

REFERENCES.

C-1. Chang, F.K. and Chang, K.Y., "Post-Failure Analysis of Bolted Composite Joints in Tension or Shear-Out Mode Failure," *Journal of Composite Materials*, Vol. 21, pp. 809-833, 1987.

C-2. Tsai, S.W. and Wu, E.M., "A General Theory of Strength for Anisotropic Materials," *Journal of Composite Materials*, Vol. 5, pp. 58-80, 1971.

C-3. Matzenmiller, A. and Schweizerhof, K., "Crashworthiness Simulations of Composite Structures—A First Step with Explicit Time Integration," Nonlinear Computational Mechanics—A State of the Art, edited by P.W. Wriggers, et al., Springer-Verlag, 1991.

C-4. Hashin, Z., "Failure Criteria for Unidirectional Fiber Composites," *Journal of Applied Mechanics*, Vol. 47, pp. 329-335, 1980.

APPENDIX D—NUMERIC PARAMETRIC STUDY SUMMARY

Table D-1. Summary of the Parametric Studies Performed

Parameter	Baseline Value	Parametric Variation	Figure
MAT54: XT (psi)	319,000	0, 5,000, 50,000, 150,000, 250,000, 300,000, 350,000, 370,000, 400,000, 500,000, and 640,000	-
MAT54: XC (psi)	213,000	0, 100,000, 150,000, 200,000, 230,000, 250,000, 265,000, 275,000, and 300,000	20
MAT54: SC (psi)	22,400	1, 10,000, 15,000, 175,000, 18,000, 19,000, 20,000, 30,000, 35,000, and 50,000	21
MAT54: YT (psi)	7,090	0, 3,000, 6,800, 7,500, 10,000, 50,000, and 500,000	-
MAT54: YC (psi)	28,800	0, 5,000, 15,000, 25,000, 30,000, 35,000, 70,000, 200,000, 288,000, 320,000, 400,000, and 500,000	22
MAT54: DFAILT (in./in.)	0.0174	0, 0.005, 0.00625, 0.00688, 0.0075, 0.01, 0.015, 0.04, and 0.08	23
MAT54: DFAILC (in./in.)	-0.0116	0, -0.005, -0.0075, -0.00813, -0.00875, -0.01, -0.012, -0.015, -0.02, -0.0225, -0.025, -0.03, and -0.1	24-25
MAT54: DFAILM (in./in.)	0.024	0, 0.01, 0.015, 0.0163, 0.0165, 0.018, 0.02, 0.03, and 0.06	26
MAT54: DFAILS (in./in.)	0.03	0, 0.006, 0.01, 0.037, 0.05, and 0.1	-
MAT54: EFS (in./in.)	0	0.005, 0.01, 0.5, and 1	27
MAT54: ALPH	0.3	0, 1.00E-14, 1.00E-6, 1.00E-4, 1.00E-3, 0.03, 0.9, and 1	28
MAT54: BETA	0.5	0 and 1	-
MAT54: FBRT	0.5	0, 0.1, 0.95, and 1	-
MAT54: YCFAC	1.2	0, 0.5, 2, 4, 7.396, and 9	-
MAT54: TFAIL	0.115E-08	0, 1E-07, 0.05, and 0.11	-
MAT54: SOFT	0.57	-0.5, 0, 0.05, 0.4, 0.55, 0.565, 0.575, 0.6, 0.8, 0.95, and 2	29
Contact type	Entity	Rigid Nodes to Rigid Body, Automatic Surface to Surface, and Eroding Surface to Surface	30-31
Contact load-penetration curve	PCWL	PCWL Stiff, PCWL Soft, and Linear	32-35
Trigger thickness (in.)	0.01	0.005, 0.015, 0.020, 0.025 0.030, 0.035, 0.040, 0.045, 0.047, 0.050, 0.060, and 0.079	36-37
Trigger geometry	Constant thickness	Tapered thickness	38
Mesh size (in.)	0.1	0.05, 0.15, and 0.2	39-40
Crush velocity (in./sec)	150	1.5, 15, and 50	41-42
SAE CFC filter	600	180 and 1,000	43